Christian-Albrechts-Universität zu Kiel

Mathematisch-Naturwissenschaftliche Fakultät

GEOMAR Helmholtz-Zentrum für Ozeanforschung Kiel

Diurnal cycle of near-surface shear, stratification and mixing in the equatorial Atlantic

Thesis

Master of Science Programme

Climate Physics: Meteorology and Physical Oceanography

by

Anna Christina Hans

1103867

Advisor: Prof. Dr. Peter Brandt

Co-Advisor: Prof. Dr. Martin Claus

Kiel, June, 2022

Contents

Abstract

The diurnal behaviour of near-surface shear, stratification and turbulent kinetic energy dissipation is examined in the equatorial Atlantic. These processes are important to consider as they modify the near-surface heat and momentum budgets. In particular, they are relevant for understanding air-sea fluxes and the vertical distribution of shear, and hence, also for improving turbulence parameterisations. In this study the respective parameters are analysed using observational data obtained from the TRATLEQ1 cruise, a glider mission, Argo floats and CARTHE as well as SVP surface drifters in the equatorial Atlantic.

The results reveal a diurnal cycle for shear, stratification and turbulent kinetic energy dissipation in the upper 2 m to 6 m of the ocean which is up to one order of magnitude stronger and sets in several hours earlier than the deep diurnal cycle below about 10 m to 20 m depth. This leads, among others, to diurnal differences in the dissipation of wind energy close to the surface. Considering 1 m instead of 15 m velocities also increases the daily mean wind power input into the ocean by 39%. Furthermore, it is shown that the wind speed has an influence on the buildup of the diurnal warm layer and the diurnal jet. A pronounced diurnal warm layer forms for wind speeds below $\sim 6\ \mathrm{m\,s^{-1}}$. The appearance of the diurnal jet changes for low ($0-3\ \mathrm{m\,s^{-1}}$), moderate ($4-6\ \mathrm{m\,s^{-1}}$) and high ($8-12\ \mathrm{m\,s^{-1}}$) wind speeds. Following the seasonality of trade winds at the equator, the near-surface shear and stratification show seasonal patterns. As the presence of shear-instabilities is governed by the ratio of shear and stratification, a seasonality for turbulent kinetic energy dissipation is expected as well.

Zusammenfassung

Der tägliche Verlauf von der Scherung, der Schichtung und der Dissipation turbulenter kinetischer Energie wird nahe der Meeresoberfläche im äquatorialen Atlantik untersucht. Die Berücksichtigung dieser Prozesse hat einen Einfluss auf die Wärme- und Impulsbilanz nahe der Meeresoberfläche. Die Prozesse sind insbesondere für das Verständnis von Flüssen zwischen Atmosphäre und Ozean relevant sowie für das Verständnis von der vertikalen Verteilung der Scherung. Damit können sie zur Verbesserung der Parametrisierungen von Turbulenz beitragen. In dieser Studie werden die entsprechenden Parameter anhand von Beobachtungsdaten analysiert, die während der TRATLEQ1 Messfahrt, einer Gleitermission sowie von verschiedenen driftenden Messinstrumenten (Argo, CARTHE, SVP) aufgenommen wurden.

Die Ergebnisse zeigen für die Scherung, die Schichtung und die Dissipation turbulenter kinetischer Energie einen Tagesgang in den oberen 2 m bis 6 m auf, der bis zu einer Größenordnung stärker ist und mehrere Stunden früher einsetzt als der Tagesgang unterhalb von 10 m bis 20 m. Unter anderem resultiert der Tagesgang in tägliche Unterschiede bei der Dissipation von Windenergie nahe der Oberfläche. Das Inbetrachtziehen von 1 m anstelle von 15 m Strömungen führt durch den zusätzlichen Tagesgang zu einer Erhöhung des täglichen mittleren Windenergieeintrags in den Ozean von 39%. Darüber hinaus wurde verdeutlicht, dass die Windgeschwindigkeit einen Einfluss auf den Aufbau der täglichen Schichtung und Scherung an der Oberfläche hat. Eine Schwelle von $\sim 6\ \mathrm{m\,s^{-1}}$ wird vorgeschlagen, die für die Bildung einer ausgeprägten Schichtung unterschritten werden muss. Die Erscheinung der täglichen Scherung ändert sich mit niedrigen ($0-3\ \mathrm{m\,s^{-1}}$), mittleren ($4-6\ \mathrm{m\,s^{-1}}$) und hohen ($8-12\ \mathrm{m\,s^{-1}}$) Windgeschwindigkeiten. Ausgehend von der Saisonalität der Passatwinde am Äquator zeigen auch die Schichtung und die Scherung nahe der Oberfläche einen saisonalen Verlauf. Da das Auftreten von Scherungsinstabilitäten durch das Verhältnis von Scherung und Schichtung bestimmt wird, wird auch ein saisonaler Verlauf für die Dissipation turbulenter kinetischer Energie erwartet.

1. Introduction

Many processes close to the ocean surface vary with the diurnal cycle of solar radiation, including stratification, shear and mixing. In that course, heat and wind forced momentum can be trapped at the surface and transmitted into the interior via a daily descending shear layer (Masich et al., 2021). The wind power input (WPI) is a measure of transferred kinetic energy, of which about 1% is used for turbulent kinetic energy (TKE) dissipation in the mixed layer (ML) (Moum and Caldwell, 1985; Sutherland et al., 2013). The daily formation of near-surface ocean stratification also modifies heat fluxes through the air–sea interface, turbulence dissipation in the ML, and the vertical profile of lateral transport (Hughes et al., 2020). Therefore, the near-surface diurnal cycle influences near-surface heat and momentum budgets. This is of particular interest close to the equator since the diurnal cycle reaches deeper in the equatorial region compared to the extratropics (Hughes et al., 2020).

Improving the understanding of processes governing near-surface heat and momentum budgets and especially the turbulent vertical flux of wind driven momentum is important for accurately modelling near-surface currents (Smyth et al., 1996). It is also crucial for energetically consistent ocean models, which are in better agreement with hydrographic observations than non-consistent models (Eden et al., 2014; Gutjahr et al., 2021). Besides, the choice of the vertical mixing scheme plays a role for regional biases in models (Gutjahr et al., 2021) and influences the simulation of future climate states (Deppenmeier et al., 2020). The inability of models to constrain turbulent mixing realistically might explain the long-standing bias in modelling sea surface temperature (SST) in the equatorial cold tongues (Jouanno et al., 2011). Observations show that including the diapycnal heat flux and boreal summer cooling via mixing can balance the seasonal ML heat budget (Hummels et al., 2014; Moum et al., 2013), though the diurnal cycle of turbulent cooling at the base of the ML seems to have no rectification onto the mean turbulent cooling (Foltz et al., 2020). However, finescale parameterisations of turbulent dissipation and diapycnal mixing are still spanning an order of magnitude or more (Polzin et al., 2014) and thus need better understanding.

1.1. Upper ocean diurnal cycle

The diurnal cycle of solar radiation (Fig. 1 (a)) induces sea surface warming from early morning until midafternoon, forming a diurnal (buoyantly isolated) warm layer (DWL) (Fig. 1 (c)). Wind vertically transfers momentum into the ocean which is then trapped in the DWL, creating a highly sheared near-surface diurnal jet (Fig. 1 (b)). During late afternoon and evening, the stratified shear layer descends, leaving

the nocturnal ML above it. The nocturnal ML is characterized by sea surface cooling and convective overturning which destroys the DWL (Price et al., 1986; Smyth et al., 2013; Masich et al., 2021). With the diminishing surface buoyancy flux, dynamic stability is lost (Smyth et al., 2013). The descending shear layer can decrease the near-surface Richardson number (Ri), moving towards shear-instability (Fig. 1 (d)). These instabilities trigger deep diurnal mixing with a lag of typically 2–3 hours (Fig. 1 (e)). Late at night, the resulting turbulence suppresses further instabilities and decays in the morning while the upper ocean restratifies (Price et al., 1986; Smyth et al., 2013).

The diurnally-varying turbulence beneath a well-mixed nighttime surface layer is termed deep cycle turbulence (e.g. Moum et al., 2022). This deep cycle was first discovered during the Tropical Heat experiment at $0°\mathrm{N}, 140°\mathrm{W}$ in 1984 with TKE dissipation rates (ϵ) ranging over two orders of magnitude, from 10^{-8} to 10^{-6} $\mathrm{W\,kg^{-1}}$ (Moum et al., 1989; Peters and Gregg, 1988). It has been mainly studied in the Pacific in the course of observations (Moum et al., 1989; Peters and Gregg, 1988; Price et al., 1986; Smyth et al., 2013; Pham et al., 2017; Smyth et al., 2021; Masich et al., 2021) and with simulations (Pham et al., 2013, 2017; Hughes et al., 2021). Yet, deep cycle turbulence is also present in the Atlantic (Sutherland et al., 2016; Moum et al., 2022). The development of small-scale geophysical turbulence is governed largely by the competition between the vertical shear of the background flow and buoyancy forces due to ambient density stratification. The vertical shear supplies the kinetic energy for turbulent motion whereas buoyancy force reduces turbulence (Smyth and Moum, 2000). The nocturnal mean value of ϵ in the deep cycle can be parameterised as $\epsilon = \rho_0^{-1} \times \boldsymbol{\tau} \times \boldsymbol{S}$, where ρ_0 is a characteristic water density, $\boldsymbol{\tau}$ the wind stress and $\boldsymbol{S}$ the horizontal shear (Smyth et al., 2019).

Considering the diurnal cycle close to the equator is particularly important as the diurnal jet only reaches up to $10 - 15$ m in the extratropics (Hughes et al., 2020) compared to about 60 m in the equatorial ocean (Masich et al., 2021). This discrepancy arises largely due to the turning of horizontal velocities with depth associated with Coriolis rotational effects (Hughes et al., 2020). Therefore, the near-surface daily heat and momentum mix far deeper into the ocean near the equator than away from it (Masich et al., 2021). Note that a correct parameterisation of the turbulent eddy viscosity is also specifically important at low latitudes where diminished rotational constraints increase the sensitivity of modeled currents and SST to vertical mixing (Schneider and Müller, 1994). Besides, the equatorial region is characterized by its zonal current system and by a highly sheared Equatorial Undercurrent (EUC). Thus for the upper equatorial ocean, it is typical that shear and stratification vary almost

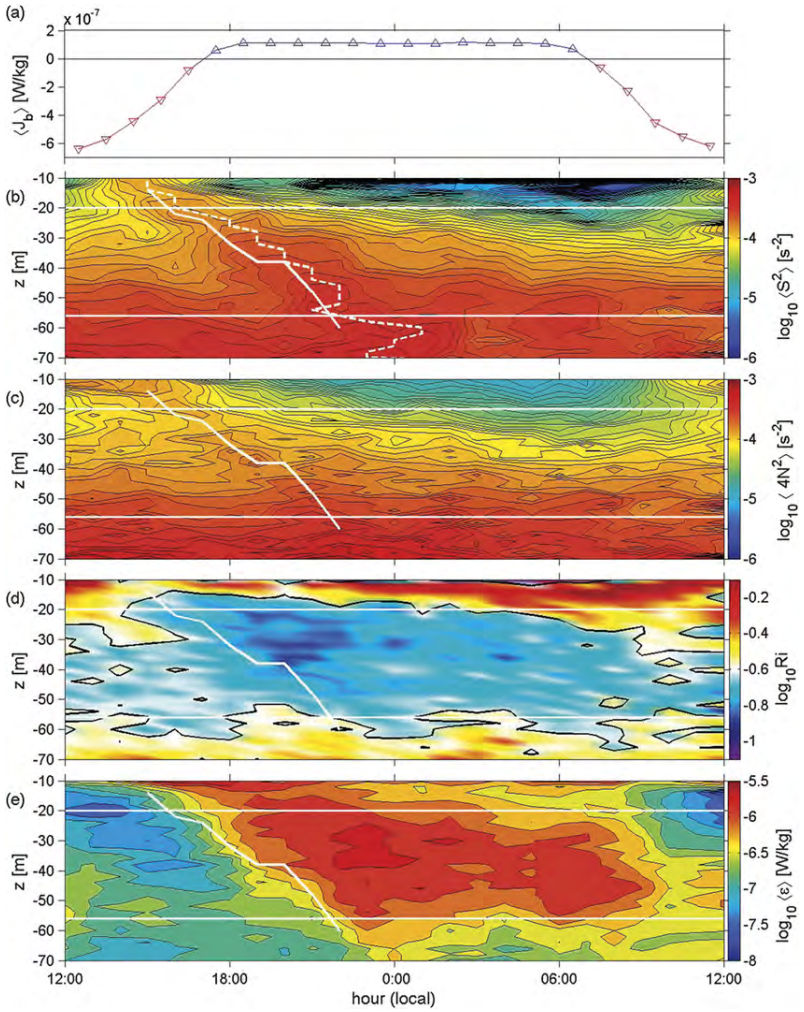

Figure 1: Diurnal cycle in the upper equatorial Pacific at $0°\mathrm{N}, 140°\mathrm{W}$ in October/November 2011 for (a) surface buoyancy flux, (b) squared horizontal shear, (c) four times the squared buoyancy frequency (The factor 4 is chosen so that shear and stratification are the same color when $\mathrm{Ri} = \frac{1}{4}$), (d) Ri, where the black contour represents $\mathrm{Ri} = \frac{1}{4}$, and (e) TKE dissipation rate. Further, the solid white curve indicates the shallowest local maximum shear with respect to depth. The white horizontal lines indicate $z = -20$ m and -56 m for reference. Taken from Smyth et al. (2013).

proportionally so that Ri remains near its critical value, a state which is termed marginal instability (Smyth and Moum, 2013; Smyth et al., 2019). This statistical equilibrium may indicate regimes in which deep cycle turbulence is active (Smyth and Moum, 2013; Thorpe and Liu, 2009). Deep cycle mixing is then triggered by instabilities formed when the descending shear layer merges with the marginally unstable shear of the EUC (Smyth et al., 2013).

Additionally, the wind force influences the near-surface diurnal cycle in the ocean, though the diurnal cycle in wind can be neglected as it is at least an order of magnitude smaller than the overall wind signal magnitude, if present at all (Masich et al., 2021; Smyth et al., 2013). According to a simulation at $18°\mathrm{N}, 126°\mathrm{E}$, a DWL forms for low winds ($\leq$ 2 $\mathrm{m\,s^{-1}}$) but shear in the near-surface jet remains too weak to generate shear-instability and mixing then. For high winds ($\geq$ 8 $\mathrm{m\,s^{-1}}$), surface heat is rapidly mixed downward and a DWL does not form. For moderate winds ($3 - 5$ $\mathrm{m\,s^{-1}}$), the near-surface jet persists for several hours and is susceptible to shear-instability with the upper 2 m being characterized by $\mathrm{Ri} \approx 0.1$ between 10:00 and 16:00 local time (LT). However, shear-instabilities only grow and mix when convective cooling starts and the region of unstable flow moves downward (Hughes et al., 2021). As wind-driven mixing determines the seasonal modulation of diurnal SST amplitudes, the near-surface diurnal cycle shows different patterns for seasons with relatively steady trade winds and those with weaker and more variable winds (Wenegrat and McPhaden, 2015).

For maximum wind speeds in boreal summer and autumn, the shear velocity between 3.75 m and 20 m reaches a maximum of 20 $\mathrm{cm\,s^{-1}}$ at 15:00 LT at $0°\mathrm{N}, 23°\mathrm{W}$. The near-surface layer is well mixed with deep ML and thermocline, leading to a layer with marginal instability of the upper EUC (Wenegrat and McPhaden, 2015). For wind speeds dropping in boreal winter and spring, the near-surface stratification and the diurnal SST amplitude increase. A shallow EUC leads to a still highly sheared near-surface layer but without a significant diurnal pattern or marginal instability (Wenegrat and McPhaden, 2015). Even if marginal instability cannot be detected throughout the year, deep cycle mixing is evident all year and the maximum turbulence levels remain relatively stable (Pham et al., 2017). However, Wenegrat and McPhaden (2015) proposed lower TKE dissipation rates for March to May applying the mixing parameterisation by Kunze et al. (1990). In the Pacific, observations indicate that changes in wind stress force a semiannual variation of the deep cycle with a boreal spring minimum and a shorter and less pronounced boreal autumn minimum (Smyth et al., 2021).

1.2. Seasonality in the equatorial Atlantic

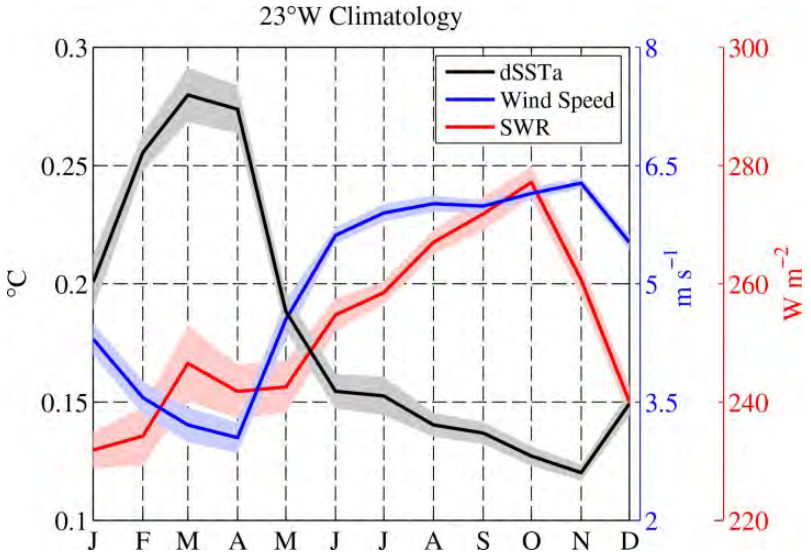

Figure 2: Monthly averaged climatology at 0°N, 23°W for diurnal SST amplitude at 1 m depth (black line), wind speed at 4 m height (blue line), and shortwave radiation at 3.5 m height (red line). Shading denotes ±1 standard error of the monthly mean. Taken from Wenegrat and McPhaden (2015).

The equatorial Atlantic velocity field is characterized by alternating westward and eastward flowing currents (Maximenko et al., 2009). At the equator, the South Equatorial Current (SEC) flows westward on top of the eastward flowing EUC which is driven by the basin-wide zonal pressure gradient set up by the westward wind stress. This zonal pressure gradient also yields an upward slope from west to east of the thermocline, in which the core of the EUC is embedded (Hormann and Brandt, 2007).

Seasonal variations in the equatorial Atlantic are induced by the meridional migration of the Intertropical Convergence Zone (ITCZ) with the apex of the sun's motion and the associated changes in the wind field, especially the one of the western basin (Lumpkin and Garzoli, 2005). In boreal summer and autumn (ITCZ away from the equator), relatively steady trade winds and clear skies lead to a deep ML and thermocline with a EUC core located at about 80 m at 0°N, 23°W. In boreal winter and spring (ITCZ approaching the equator), weaker trade winds along with frequent cloudiness and precipitation produce a shallow ML and thermocline and with a EUC core at about 50 m at 0°N, 23°W with its upper limbs reaching up to 15 m (Brandt et al., 2014; Wenegrat and McPhaden, 2015). A climatology from the PIRATA (Prediction and Research Moored Array in the Atlantic) buoy at 0°N, 23°W produces this seasonal cycle in wind with minimum winds at 4 m height in April of, on average, 3 $\mathrm{m\,s^{-1}}$ and maximum ones in July to November of 3 $\mathrm{m\,s^{-1}}$. This seasonal cycle of wind speed correlates well with the inverted amplitude for the diurnal cycle of

the temperature at 1 m depth (Fig. 2). Cooling through vertical mixing exhibits a semiannual cycle in the equatorial Atlantic with one peak in May to June and one peak in November to December. These events are closely linked to the enhancement of the vertical shear just above the core of the EUC (Jouanno et al., 2011).

1.3. Near-surface diurnal cycle

Typically, near-surface ocean currents and turbulence are measured below 10 m depth, which can be below the DWL. Even though there have been advances in measurements (Wenegrat and McPhaden, 2015; Moum et al., 2022; Hughes et al., 2020), the upper 10 m are still undersampled. Yet, to assess air-sea fluxes it is relevant to also consider processes in these upper meters. Besides, to evaluate turbulent energetics in the ML, a more accurate description of vertical shear in the ML is necessary. This is the case especially since a large but unknown fraction of this atmospheric energy is dissipated by turbulence in the upper ocean while numerous studies have failed to converge on the same scaling for TKE dissipation rates (Zippel et al., 2022). While recent parameterisations of the turbulent eddy viscosity and of the effect of turbulent momentum mixing depend on the wind stress and current shear, previous parameterisations depended on the wind stress only (Wenegrat et al., 2014; Smyth et al., 2021). This stresses again the importance of knowing the vertical shear. Moreover, the strength of the TKE dissipation does not only affect physical properties and climate modelling as described earlier, but also affects estimates of the air–sea transfer of water soluble gases, such as carbon dioxide (CO_2) or oxygen (O_2) (Zappa et al., 2007). Following from that, the motivation of this study is to examine the diurnal behaviour of shear, stratification and mixing close to the surface in the equatorial Atlantic.

The thesis is structured as follows: In section 2, the datasets used for this study and the methods applied are described. Then, the shear between 1 m and 15 m currents is investigated in section 3.1. Measurements for stratification and TKE dissipation from 2 m depth downwards are presented in sections 3.2 and 3.3 respectively. The influence of wind on shear and stratification and the resulting seasonality is analysed in sections 3.1 and 3.2. Furthermore, the TKE dissipation is compared to the WPI in section 3.4. The mixing parameterisation by Kunze et al. (1990) is used in section 3.5 to estimate the shear between 2 m and 6 m depth.

2. Data and Methods

2.1. Data

This study focuses on different in-situ measurements in the Eulerian framework from research vessels and gliders as well as in the Lagrangian framework from surface drifters and Argo floats. Additionally, a remote sensing satellite dataset is used. In the following, the applied datasets are described.

2.1.1. Cruise TRATLEQ1

Shipboard measurements from the cruise M158 with the research vessel Meteor are used. The so called *Trans-Atlantic Equatorial Cruise 1* (TRATLEQ1) measured the Atlantic equatorial transect from east to west between September 29, 2019 and October 22, 2019. In the following, the instruments used here are described.

Radar A coherent-on-receive, marine X-band (9.4 GHz) Radar developed at the Helmholtz-Zentrum Geesthacht measured the spectral quantities of ocean surface waves. The instrument was set to operate at a pulse length of 80 ns (i.e. short-pulse mode), providing a range resolution of 7.5 m. It is equipped with a 2.3 m (7.5 ft) horizontal transmit and receive (HH)-polarised antenna having a rotational period of 2 s and a pulse repetition frequency of 2 kHz. The horizontal antenna beam width is 1.1°. The obtained image sequences are analysed with respect to long surface wave properties. The surface velocity can then be derived from the difference between the resulting phase velocity and the phase velocity given by the theoretical dispersion relation (Horstmann et al., 2015). For such, a mean penetration depth of 1 m is assumed. However, the actual penetration depth varies depending on the surface wave length. Only data between 0.01°S and 0.01°N are considered. There are no data between 18°W and 25°W, i.e. October 09 to October 12, 2019.

vmADCP Current information was obtained from the vessel mounted Acoustic Doppler Current Profiler (vmADCP), a 75 kHz RDI Ocean Surveyor. It was configured with 100 bins of 8 m and a blanking distance of 4 m, reaching a range of $600 - 700$ m. Here, only data from the uppermost bin at 17 m are considered.

Thermosalinograph Underway measurements of sea surface temperature (SST) and practical sea surface salinity were continuously made by the ship's dual thermosalinograph (TSG). Here, the 1 min calibrated data for salinity is used as well as the 10 s uncalibrated data for temperature. Additionally, the 10 s pitch and the 10 s roll from the ship are taken.

Microstructure A MSS90-DII microstructure profiler of Sea and Sun technology was used which was equipped with three airfoil shear sensors to infer TKE dissipation rate assuming isotropic turbulence. The probe was loosely tethered and thus quasi free-falling with a sink velocity of about $0.55\,\mathrm{m\,s^{-1}}$. In total, 107 profiles at 35 stations were taken along the equator. The raw data were converted to usable data by automatic processing routines. The processing algorithm is described in more detail in Schafstall et al. (2010). Afterwards, corrupted data points were removed by a manual despiking. Data collected in the upper 15 m are neglected due to ship induced turbulence.

Wind Wind speed and direction from the meteorological shipboard measurements at ~ 30 m height are considered. These data have a temporal resolution of 1 min.

2.1.2. Glider data

The autonomous glider deepy (ifm02) manufactured by Teledyne/Webb Research was deployed at $0°\mathrm{N}, 10°\mathrm{W}$ by the research vessel Maria S. Merian during the cruise MSM18/2 and recovered during MSM18/3. The deployment (no. 16) lasted from June 13, 2011 to July 09, 2011. Deepy was programmed to circle the PIRATA buoy at $0°\mathrm{N}, 10°\mathrm{W}$ and took 287 profiles in total. The attached Seabird CTD system measured conductivity, temperature and pressure from which practical salinity could be derived. The glider was further equipped with a MicroRider microstructure instrument package by Rockland Scientific which includes two airfoil shear sensors, two fast thermistors and a SeaBird micro-conductivity sensor. Accelerometers recorded pitch, roll and heave of the system. A flight model (Merckelbach et al., 2019) is used to estimate the horizontal speed of flow past the sensors. This is required for processing microstructure shear and temperature measurements since the flow speed cannot be determined from the rate of change of pressure as usually done for free-falling vertical profilers. An automatic processing from 2014 derived the TKE dissipation rate assuming isotropic turbulence using a threshold glider speed of $0.1\,\mathrm{m\,s^{-1}}$. Allowing lower glider velocities around the turning points would lead to noisier data and underestimated turbulence for less force at the shear sensors. Additionally, turbulence data were despiked by-hand for June 25, 2011 til June 29, 2011. One shear sensor failed at July 01, 2011, so the turbulence data from both sensors are considered only until then. Furthermore, it should be noted that the salinity data from the CTD contained artefacts close to the surface. They are a result from the unknown time lag in measuring temperature and conductivity. Especially at the turning points the estimate of the time lag is error-prone.

2.1.3. Surface drifters

The Global Drifter Program maintains a global array of satellite-tracked surface drifters, the so called Surface Velocity Program (SVP) drifters. They consist of a spherical surface buoy tethered to a weighted holey-sock drogue that allows the drifters to follow currents at a nominal depth of 15 m. This study uses the hourly interpolated dataset by Elipot et al. (2016). Trajectories from Argos and GPS tracked drifters are interpolated to hourly intervals for gaps smaller than 12 h. Further, a quality control is performed to remove spurious data and to assess the status of the drogue. For the region 10°S to 10°N in the tropical Atlantic about 2×10^6 drifter measurements were available from July 28, 2000 to April 06, 2020 with in-homogeneous spatial and temporal distribution. It should be noted that surface drifters do not follow the currents perfectly but have a slip bias of less than 1 $\mathrm{cm\,s^{-1}}$ in 10 $\mathrm{m\,s^{-1}}$ winds according to observations. This bias results from the direct action of the wind on the surface floating buoy as well as from the vertical shear of the horizontal velocity across the vertical extent of the drogue (Niiler et al., 1995).

During the TRATLEQ1 cruise, the TRATLEQ1 drifter experiment was carried out where 31 SVP drifters (drift at 15 m depth) and 27 CARTHE (Consortium for Advanced Research on Transport of Hydrocarbon in the Environment) drifters (drift at 0.6 m $\approx$ 1 m depth) were deployed along the equator between September 29, 2019 and October 18, 2019 (Hans and Brandt, 2021). 91% of the collocated values were obtained in October 2019. This dataset is described in more detail in appendix A.

2.1.4. Argo floats

The Argo program maintains a global array of autonomous profiling floats that can change their buoyancy by pumping water in and out of an external bladder. The floats perform cycles of about 9.5 days, consisting of vertical profiles, drift at parking depth and drift at the surface. During the surface drift data are transmitted. As transmission improved during the last 20 years, the surface time of the Argo floats decreased (Fig. 3). Here, the YoMaHa'07 dataset (Lebedev et al., 2007) is used which assesses trajectories of Argo floats at parking level and at the sea surface. From the latter, surface velocities (drift at $\sim$ 1 m depth) are calculated by a linear least square regression method yielding one surface velocity value per cycle. Thus, the sampling time at the surface limits the resolvable velocity frequencies. Therefore, only surface times smaller than 6 h are considered to be able to reproduce a diurnal cycle. For the region 10°S to 10°N in the tropical Atlantic about 5×10^4 Argo surface velocities were available from July 28, 1997 to October 23, 2021 with in-homogeneous spatial and temporal distribution.

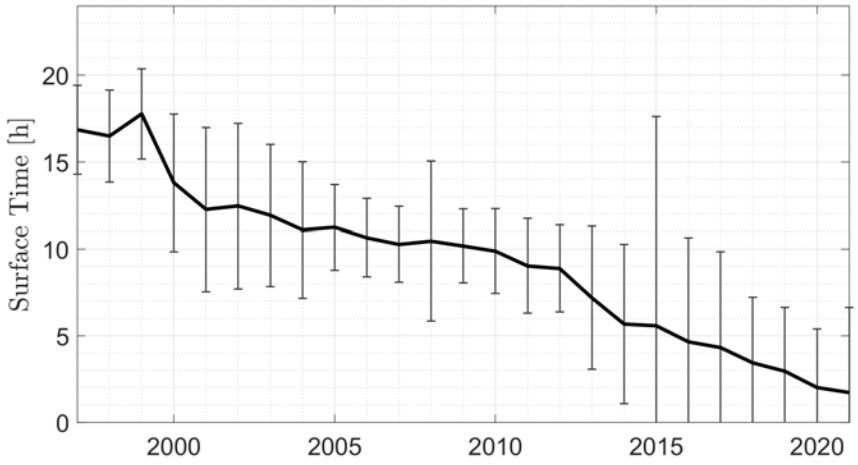

Figure 3: Annual mean surface time per cycle of Argo floats from 1997 to 2021.

2.1.5. Satellite wind

The gridded 6 hourly CCMP NRT wind satellite product provided by REMSS was used to get long-term data from January 2000 to May 2020 for winds at 10 m height. The product is processed to L3 standard and has a resolution of 0.25° x 0.25° x 6h (Wentz et al., 2015). More information can be found at http://www.remss.com/measurements/ccmp/.

2.2. Methods

2.2.1. Solar Apparent Time

Diurnal cycles are computed in Solar Apparent Time (SAT). This is a longitudinal correction of the Coordinated Universal Time (UTC) to local time so that solar noon is centered at 12:00. Additionally, the equation of time is used to correct from the mean to apparent time, taking the declination of the sun into account and thus, the displacement of solar central meridian passage from solar noon. Times are converted from UTC to SAT using the Matlab function UTC2SolarApparentTime(UTC,Lon) by Koblick (2021).

2.2.2. Shear

The horizontal shear is defined as $S^2 = u_z^2 + v_z^2$, where u_z and v_z are the vertical derivatives of the zonal and meridional velocities. For shear of the TRATLEQ1 equatorial transect between Radar and the uppermost bin of the vmADCP, 10 min averages were calculated. Outliers of the resulting shear values were eliminated using a criterion of 3 standard deviations off the median. Applying this criterion does not generate a bias in the hour of the day and thus presumably does not remove true

high values. The computation of shear for the TRATLEQ1 drifter experiment is described in appendix A.
The shear between Argo surface drift and SVP drifters is calculated for both collocated and uncollocated datasets. For collocation a distance criterion of $\triangle\text{lat} = 1°$ and $\triangle\text{lon} = 5°$ and a time criterion of $\triangle\text{time} = 1$ h is used. For the longitudinal criterion, $\triangle\text{lon} = 5° \approx 500$ km is considered to still be smaller than horizontal scales of tropical instability waves (which are often described as undulations of the seasonal SST) of about $600 - 1200$ km (Steger and Carton, 1991). A criterion of 3 standard deviations off the median is applied to remove outliers as this does not yield a diurnal bias. This leads to 12,023 collocated shear values for 10°S to 10°N from 2000 until 2020. For the equatorial region (2°S to 2°N) there are only 1,706 collocated shear values from 2000 until 2020. Due to limited amount of values at the equator, only uncollocated data were considered for the following results. For uncollocated data, the seasonal mean is removed for both Argo and SVP velocities. It was derived from the monthly 1° horizontally resolved SVP climatology, cubically interpolated to daily values. The cubical interpolation was chosen to avoid errors in the variance which would have been the case for linear interpolation.

Along and across wind component The zonal and meridional ocean velocities are transformed to along and across wind components by rotation, as follows:

$$U_{along} = u \times cos(\varphi) + v \times sin(\varphi) \qquad U_{across} = -u \times sin(\varphi) + v \times cos(\varphi) \qquad (1)$$

where u, v are zonal and meridional ocean velocities and φ describes the angle between the wind vector and the original coordinate system. Positive U_{across} correspond to velocities to the left of the wind direction. The chosen wind value is always the one closest in time and space to the satellite wind.

Diurnal cycle fit Due to the limited number of observational data, a linear fit is applied for some analysis, so that only 5 instead of 24 parameters are needed to determine the diurnal cycle. The data are fitted to sine and cosine functions for a diurnal (a_n) and a half diurnal (b_n) cycle plus the mean (c):

$$diurnal\,fit\,(t) = a_1 sin(\frac{2\pi}{24h}t) + a_2 cos(\frac{2\pi}{24h}t) + b_1 sin(\frac{2\pi}{12h}t) + b_2 cos(\frac{2\pi}{12h}t) + c \quad (2)$$

where t is the time of the day in hours.

Uncertainty quantification of the fit In order to determine the accuracy of the diurnal fits, the bootstrapping method is utilised. This allows to establish confidence intervals for the estimated parameters without prior knowledge of the shape of the

underlying distribution (Efron, 1979). For each diurnal fit, 10,000 resamples are taken from the original dataset with replacement and equal probability for each datapoint to be selected. Each resample set has the sample size of the original dataset. From the resulting distribution of parameters for the diurnal fit, a 95% confidence interval (CI) is given by taking the 2.5% and 97.5% quantiles.

2.2.3. Stratification

Derived from the TSG The stratification at the depth of the thermosalinograph inlet can be estimated using high frequency data (here 0.1 s^{-1}) for temperature and the vertical movement of the inlet position relative to the water column. This method is first described in Fischer et al. (2019). The vertical distance of the inlet relative to the mean sea level is evaluated as:

$$\begin{aligned} d_{inlet/sealevel} \approx (y_{inlet/com} \times sin(\psi) - z_{inlet/com} \times cos(\psi)) \times cos(\gamma) \\ - x_{inlet/com} \times sin(\gamma) + d_{com/sealevel} \end{aligned} \tag{3}$$

where $(x, y, z)_{inlet/com}$ are the inlet position relative to the center of mass in ship coordinates, positive for (bow, starboard, up), and $d_{com/sealevel}$ is the distance of the center of mass to sea level. For the RV Meteor III, $(x, y, z)_{inlet/com} = (40\text{ m}, -3\text{ m}, -2\text{ m})$ and $d_{com/sealevel} = 1$ m. Moreover, ψ is the roll angle positive for starboard down and γ is the pitch angle positive for bow up. This calculation is only an estimate (being accurate to at least the order) as the actual wave height and phase time series are unknown. Thus, the vertical displacement of the water column at the inlet from wave orbitals is not considered. The mean $d_{inlet/sealevel}$ during the equatorial section of TRATLEQ1 is $4.04\text{ m} \pm 0.38$ m.

The stratification is defined, according to IOC et al. (2010), as:

$$N^2 = g^2 \rho \frac{\beta \triangle S_A - \alpha \triangle \Theta}{\triangle P} \tag{4}$$

where Θ is the conservative temperature, S_A the absolute salinity, ρ the in-situ density, g the gravitational acceleration, α and β the thermal expansion and saline contraction coefficients, respectively. It should be noted that $\triangle P$ is given in Pa. Further, the stratification is determined by the density gradient with temperature variations being the main contributor to density variations. Salinity variance is neglected as there have not been rain events, i.e. $\triangle S_A = 0$. The vertical temperature gradient is given by:

$$T_z = \frac{\sqrt{var(T)}}{\sqrt{var(d_{inlet/sealevel})}} \tag{5}$$

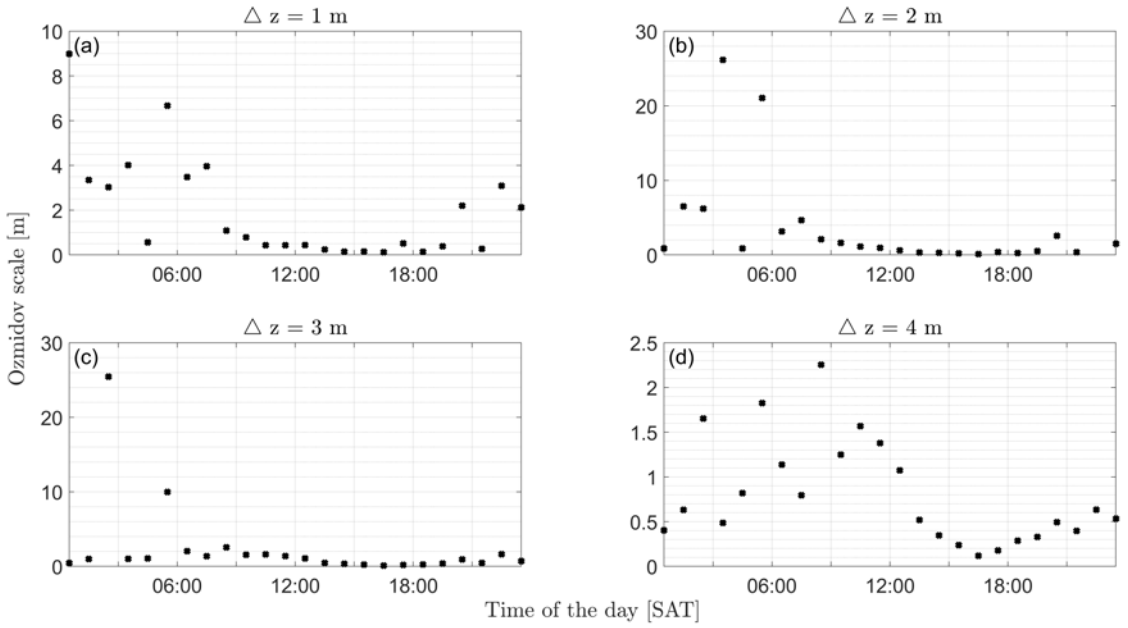

Figure 4: Hourly mean Ozmidov scale for vertical resolutions of (a) $\triangle$z = 1 m, (b) $\triangle$z = 2 m, (c) $\triangle$z = 3 m and (d) $\triangle$z = 4 m and the resulting uppermost bin derived from the glider deepy deployment no. 16.

where T is the temperature measured at the thermosalinograph inlet. The variances are calculated to a 180 s low pass filter. 180 s correspond to 1 km distance at 11 kn. Then, Eq. 4 and therewith the stratification at 4 m can be approximated to:

$$N^2 \approx -g^2 \rho \alpha \frac{\triangle \Theta}{\triangle P} \approx g^2 \rho \alpha \frac{T_z}{10^4} \tag{6}$$

The Gibbs SeaWater Oceanographic Toolbox of TEOS-10 is used for the above mentioned computations.

Derived from the glider Temperature and practical salinity data from the glider are given on an irregular pressure grid. To compute the background stratification, the vertical scale to be used needs to be larger than the Ozmidov scale $L_0 = \sqrt{\frac{\epsilon}{N^3}}$, where ϵ is the TKE dissipation rate and N the stratification. L_0 is a length scale to describe turbulent flow for steady stratification. Thus, it is the size of the largest eddy unaffected by buoyancy (Ozmidov, 1965). Analysis of hourly Ozmidov scales for different vertical resolutions close to the surface reveal $\triangle$z = 4 m as the smallest vertical scale for which $L_0 < \triangle z$ (Fig. 4). Therefore, $\triangle$z = 4 m is utilised here to calculate background stratification. In the salinity data, there are artefacts at the turning points of the glider close to the surface. Hence, the 10 m salinity is used to compute stratification in the upper 5 m for the vertical salinity gradient in the upper 10 m being negligible.

The stratification can then be calculated using Eq. 4. The respective parameters are computed using the Gibbs SeaWater Oceanographic Toolbox of TEOS-10.

2.2.4. Mixing parameterisation

Kunze et al. (1990) introduced a parameterisation for the TKE dissipation rate, hereafter called KWB. This estimate is based upon the production of turbulence by shear-instability and requires the resolution of unstable Ri:

$$\langle \epsilon \rangle = \frac{fr \times \triangle z^2}{96} \underbrace{\langle S^2 - \frac{N^2}{Ri_c} \rangle}_{(i)} \underbrace{\langle S - \frac{N}{\sqrt{Ri_c}} \rangle}_{(ii)} \tag{7}$$

where S is horizontal shear, N stratification. fr is the fraction of water occupied by unstable shear, i.e. fraction of water for which $Ri = \frac{N^2}{S^2} < Ri_c$ where Ri_c is the critical Richardson number. $\triangle z$ is the vertical derivative scale, here $\triangle$z = 4 m so that L_0 is exceeded, as explained above. The term *(i)* describes the available kinetic energy in a shear profile which is dissipated at turbulent fluxes to raise the Ri profile to Ri = $\mathrm{Ri_c}$. The term *(ii)* describes the turbulent production rate, i.e. the growth rate of Kelvin-Helmholtz billows.
The Richardson criterion is used for determining the existence of instability: $Ri = \frac{N^2}{S^2} < Ri_c$. The value of $\mathrm{Ri_c}$ may be treated as a free parameter to account for observational constraints such as vertical resolution and the ratio between shear variance and mean stratification. For $\triangle z = 4\ m$ and $\frac{\langle S^2 \rangle}{N^2} \approx 1.25$ it is appropriate to use $\mathrm{Ri_c} = 0.4$. For a higher ratio $\mathrm{Ri_c} = 0.33$ and for a lower ratio $\mathrm{Ri_c} = 0.5$ is suggested (Polzin, 1996). As there are no shear data for the considered glider mission, the ratio between shear variance and mean stratification is unknown and $\mathrm{Ri_c} = 0.4$ is used.
The KWB parameterisation can be rewritten as:

$$S^3 - \frac{N}{\sqrt{Ri_c}} \times S^2 - \frac{N}{\sqrt{Ri_c}}^2 \times S + \frac{N}{\sqrt{Ri_c}}^3 - \frac{96 \times \epsilon}{fr \times \triangle z^2} = 0 \tag{8}$$

so that S can be derived from known N and ϵ. Here $fr = 1$ for $\epsilon \neq 0$, implying that the resulting S must satisfy $S^2 > Ri_c^{-1} \times N^2$. Further, physically meaningful solutions for S need to be positive and real values.

2.2.5. Wind at 10 m height

The shipboard horizontal wind measurements in 30 m height from the TRATLEQ1 cruise are scaled to 10 m wind velocities using a logarithmic wind profile which holds for the atmospheric boundary layer. For conditions of neutral stability, the wind

profile equation is given by: (Fleagle and Businger, 1981)

$$U(z) = \frac{U_*}{\kappa} \times ln(\frac{z}{z_0}) \tag{9}$$

where U is the wind velocity at height z, U_* is the friction velocity, κ the von Karman's constant and z_0 the surface roughness length. Offshore, $z_0 = 0.0002$ m holds (Dutton, 1995). Following from that, the 10 m winds can be calculated as:

$$U(10\,m) = U(30\,m) \times \frac{ln(10\,m) - ln(z_0)}{ln(30\,m) - ln(z_0)} \tag{10}$$

2.2.6. Wind power input

The WPI is the mechanical energy transferred by winds into the ocean. It provides the energy for upper ocean turbulence. The wind stress works on the ocean flow, so that the WPI is defined as:

$$WPI = \boldsymbol{\tau} \times \boldsymbol{u} \times \rho_w^{-1} \tag{11}$$

where the wind stress $\boldsymbol{\tau}$ is given as: (Pacanowski, 1987)

$$\boldsymbol{\tau} = \rho_a \times c_D \times (\boldsymbol{u_{10}} - \boldsymbol{u}) \times |\boldsymbol{u_{10}} - \boldsymbol{u}| \tag{12}$$

Here $\boldsymbol{u}$ is the observed velocity at 1 m depth, $\boldsymbol{u_{10}}$ is the wind velocity at 10 m height, $\rho_w = 1025\ kg\,m^{-3}$ the density of water and $\rho_a = 1.223\ kg\,m^{-3}$ the density of air. The drag coefficient is calculated as $c_D = (2.717 \times |\boldsymbol{u_{10}}|^{-1} + 0.142 + 0.0764 \times |\boldsymbol{u_{10}}|) \times 10^{-3}$ (Large et al., 1995).

3. Results

In the following section the diurnal behaviour of shear, stratification and TKE dissipation in the upper equatorial Atlantic is examined, as described above.

3.1. Shear observed between 1 m and 15 m depth

During the TRATLEQ1 cruise in October 2019, shear velocities are measured between 1 m and 15 m depth by CARTHE and SVP drifters and between 1 m and 17 m depth by Radar and vmADCP (Fig. 5 (a, b)). For both datasets, shear velocities are strongest in the along wind component compared to the across wind component. Note that the mean wind direction during the TRATLEQ1 cruise was 155°, yielding winds towards north-north-west. Besides, there is a distinct diurnal cycle in the along wind but not in the across wind component. Maximum shear velocities in the along wind direction for CARTHE vs SVP are measured from 15:00 to 16:00 SAT amounting to 0.120 $\mathrm{m\,s^{-1}}$, which is associated with a shear of 0.009 $\mathrm{s^{-1}}$. For Radar vs vmADCP, maximum velocities are measured one hour earlier from 14:00 to 15:00 SAT amounting to 0.122 $\mathrm{m\,s^{-1}}$, associated with shear values of 0.008 $\mathrm{s^{-1}}$. For minimum shear velocities in the along wind direction, velocities of 0.004 $\mathrm{m\,s^{-1}}$ associated with lowest shear of 0.000 $\mathrm{s^{-1}}$ were obtained from 05:00 to 06:00 SAT with CARTHE vs SVP. At the same point in time, Radar vs vmADCP measurements reach a minimum of 0.031 $\mathrm{m\,s^{-1}}$ and associated shear of 0.002 $\mathrm{s^{-1}}$. This results in an amplitude of the diurnal shear velocities of 0.116 $\mathrm{m\,s^{-1}}$ for CARTHE vs SVP and of 0.091 $\mathrm{m\,s^{-1}}$ for Radar vs vmADCP. For shear velocities in the across wind direction, maximum absolute values of solely 0.032 $\mathrm{m\,s^{-1}}$ for CARTHE vs SVP and of 0.018 $\mathrm{m\,s^{-1}}$ for Radar vs vmADCP are reached. The respective daily means are 0.022 $\mathrm{m\,s^{-1}}$ and -0.007 $\mathrm{m\,s^{-1}}$. Accordingly, both shear datasets yield similar results, though in the along wind direction the diurnal amplitude for CARTHE vs SVP is larger than for Radar vs vmADCP due to lower values in the evening and early morning.

Shear velocities between 1 m and 15 m depth with larger temporal and spatial coverage are obtained from comparing Argo surface data and SVP data (Fig. 5 (c, d)). Here the period from 2000 to 2020 for latitudes between 2°S and 2°N is considered for all calendar months and for September to December only. For both, shear velocities are stronger in the along wind than in the across wind component. Mean shear velocities in along wind direction are 0.122 $\mathrm{m\,s^{-1}}$ for the boreal autumn period and 0.100 $\mathrm{m\,s^{-1}}$ for the whole period, associated with shear values of 0.009 $\mathrm{s^{-1}}$ and 0.007 $\mathrm{s^{-1}}$, respectively. For the across wind direction, shear velocities amount to -0.012 $\mathrm{m\,s^{-1}}$ for the boreal autumn period and -0.018 $\mathrm{m\,s^{-1}}$ for the whole period, resulting in one order of magnitude lower shear. Besides, there is a diurnal pattern

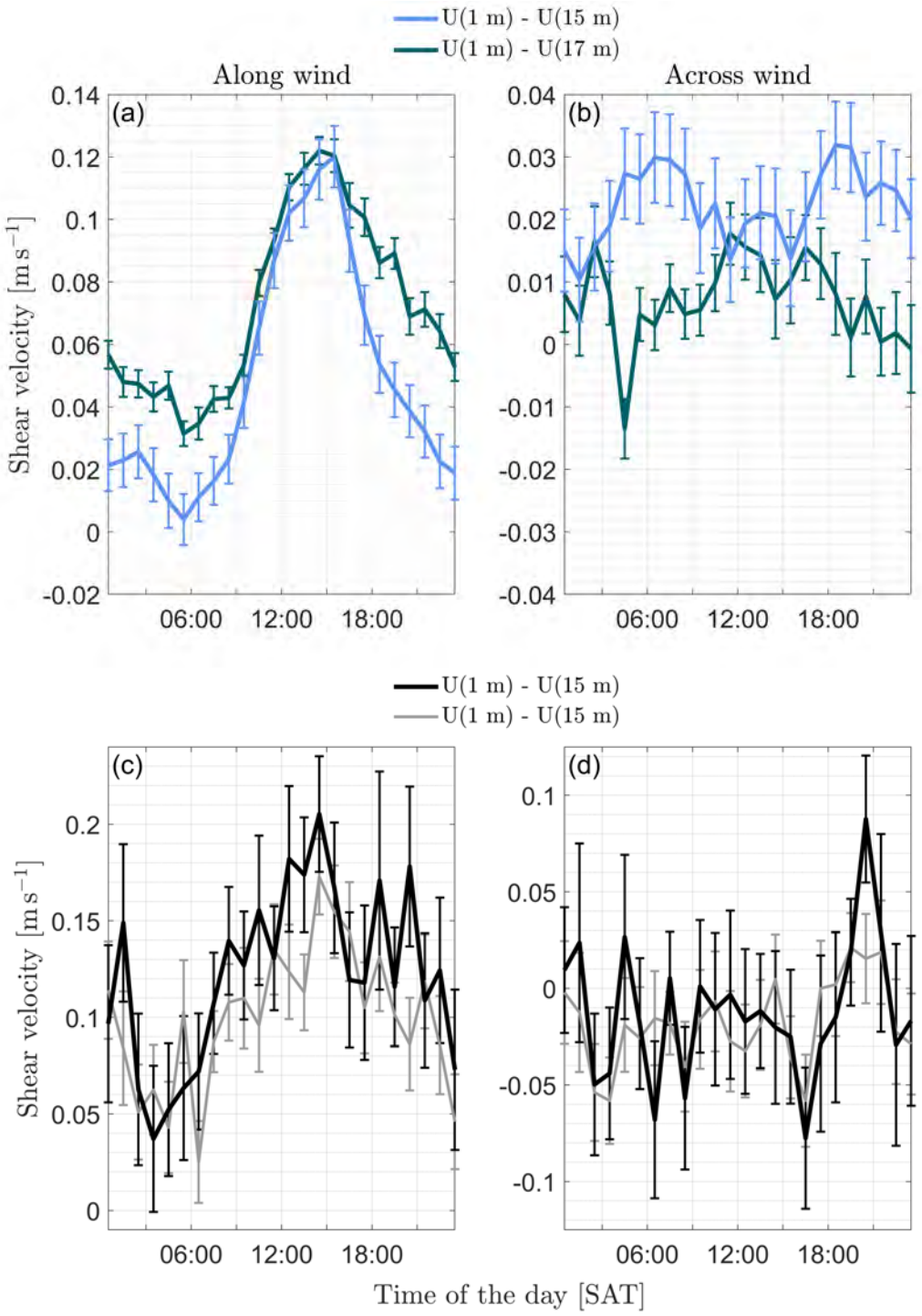

Figure 5: Diurnal cycle of shear velocities in (a, c) along and (b, d) across wind direction. The shear velocities in (a, b) are derived from the Radar and vmADCP data (dark green) acquired during the TRATLEQ1 cruise as well as from the CARTHE and SVP drifters (light blue) that were deployed during the TRATLEQ1 drifter experiment. (c, d) same as (a,b) but for the Argo surface and SVP values between 2°S and 2°N from September to December (all calendar months) during the period 2000 to 2020 in black (grey). The standard error is denoted with errorbars.

in the along wind but not in the across wind component. The diurnal cycle of shear velocities has an amplitude of 0.168 $\mathrm{m\,s^{-1}}$ for the boreal autumn period and an amplitude of 0.148 $\mathrm{m\,s^{-1}}$ for the whole period. Both periods show maximum velocities from 14:00 to 15:00 SAT and minimum velocities in the morning. This means that there is a diurnal cycle for shear velocities in the along wind component which is slightly more pronounced in the boreal autumn period compared to the whole one. Furthermore, comparing the mentioned boreal autumn period to the TRATLEQ1 measurements yields a similar pattern with the amplitude of the diurnal shear cycle in along wind direction being 43% (83%) larger than CARTHE vs SVP (Radar vs vmADCP) measurements. However for the boreal autumn period, the diurnal shear cycle in the along wind component is less distinct, smoother and afflicted with larger standard errors in contrast to the TRATLEQ1 measurements.

Seasonality The diurnal behaviour of shear in the along wind direction is examined for different seasons using a diurnal fit allowing signals at frequencies of half a day and frequencies of a day (Fig. 6). Highest afternoon shear values with about 0.014 $\mathrm{s^{-1}}$ are found in July to October (Fig. 6 (f)-(i)), corresponding to shear velocities between 1 m and 15 m depth of 0.20 $\mathrm{m\,s^{-1}}$. In January to April (Fig. 6 (l)-(d)), the afternoon shear is lowest with about 0.007 $\mathrm{s^{-1}}$, corresponding to shear velocities of 0.10 $\mathrm{m\,s^{-1}}$. Throughout the year, the hour of the diurnal afternoon peak is varying between 12:00 and 18:00 SAT with the earliest peak for September and October (Fig. 6 (h)-(i)) and the latest peak for December to February (Fig. 6 (k)-(a)). Moreover, a diurnal cycle is not noticeable all year. From May to August (Fig. 6 (d)-(g)) a pronounced half diurnal cycle going along with a narrower diurnal peak in the afternoon can be observed. In November to April (Fig. 6 (j)-(c)) the half diurnal cycle is negligible. For all months but May, the diurnal cycle is dominating the half diurnal cycle. Besides, February to May (Fig. 6 (a)-(d)) show the highest spread in shear velocity estimates from bootstrapping as well as the smallest amplitude of the diurnal cycle.

Influence of wind on shear The diurnal pattern of the along wind shear component can be compared to the wind speed (Fig. 7). The shear for all wind speeds (Fig. 7 (a)) is characterised by a clear diurnal cycle with a maximum of 0.008 $\mathrm{s^{-1}}$ from 13:00 to 14:00, a minimum of 0.002 $\mathrm{s^{-1}}$ from 05:00 to 06:00 SAT and an amplitude of 0.006 $\mathrm{s^{-1}}$. The diurnal fit for moderate winds ($4-6$ $\mathrm{m\,s^{-1}}$, Fig. 7 (c)) shows a similar pattern with a maximum at 13:00 SAT of 0.008 $\mathrm{s^{-1}}$, a minimum from 05:00 to 06:00 SAT of 0.004 $\mathrm{s^{-1}}$ and an amplitude of 0.004 $\mathrm{s^{-1}}$. For weak winds ($0-3$ $\mathrm{m\,s^{-1}}$, Fig. 7 (b)), the accuracy of the estimate is low and there is a peak for both the

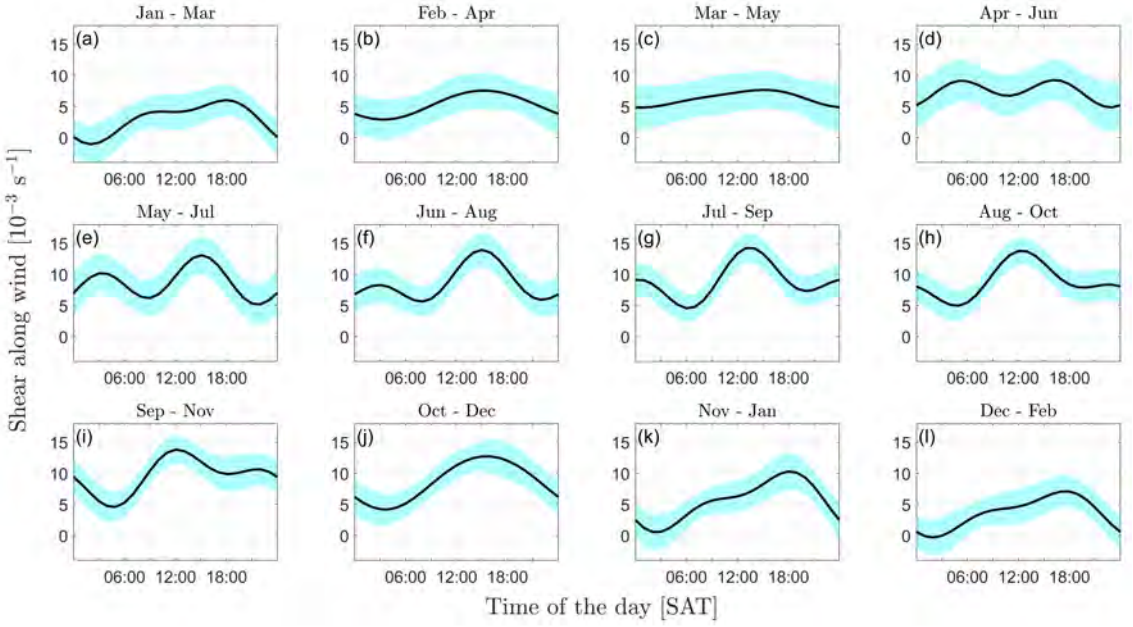

Figure 6: Diurnal cycle of the shear in the along wind direction for different seasons derived from Argo surface and SVP values between 2°S and 2°N during the period 2000 - 2020. (a)-(l) show the respective means of 3 consecutive months. The shaded areas mark the 95% confidence intervals.

diurnal and the half diurnal cycle. This implies that there is no marked diurnal cycle and that the wind is too weak to generate a diurnal jet though there is a peak between 19:00 and 20:00 SAT of 0.011 s^{-1}. In contrast to that, strong winds ($8 - 12\ m\,s^{-1}$, Fig. 7 (d)) reveal a diurnal cycle with a narrower peak compared to moderate winds. The amplitude of the half diurnal cycle is small in contrast to the one of the diurnal cycle. Moreover, the diurnal amplitude is higher for strong winds with 0.007 s^{-1} compared to moderate winds with 0.004 s^{-1}. This is because of similar strong shear in the afternoon but weaker shear in the evening and early morning for higher wind speeds. Nevertheless, the 95% CIs show a rather wide range of the diurnal estimate for strong winds, comparable to the range for weak winds. This wider range is partly caused by fewer weak and strong wind events in the dataset compared to the number of moderate wind events.

A correlation to the wind speed is neither found for the amplitude of shear, the amplitude of 1 m velocities and the amplitude of 15 m velocities, nor for the along nor the across wind component of shear, 1 m velocities and 15 m velocities. There is also no correlation considering the wind groups $0 - 4\ m\,s^{-1}$, $4 - 8\ m\,s^{-1}$, $8 - 12\ m\,s^{-1}$ separately (not shown here). However, the meridional wind stress correlates with the meridional shear obtained from Radar vs vmADCP measurements during the TRATLEQ1 cruise yielding a coefficient of 0.8. This implies that higher meridional

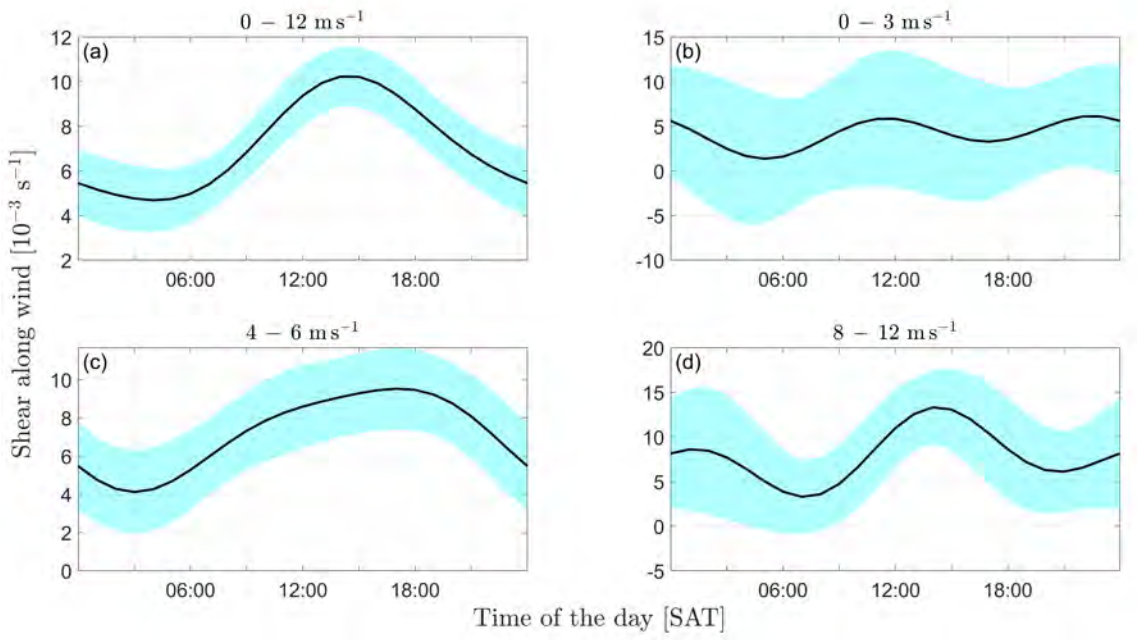

Figure 7: Diurnal cycle of the shear in the along wind direction for wind speeds of (a) $0-12\ \mathrm{m\,s^{-1}}$, (b) $0-3\ \mathrm{m\,s^{-1}}$, (c) $4-6\ \mathrm{m\,s^{-1}}$ and (d) $8-12\ \mathrm{m\,s^{-1}}$ derived from Argo surface and SVP velocities between 2°S and 2°N during the period 2000 - 2020. The shaded areas mark the 95% confidence intervals.

wind stress results in higher meridional shear close to the equator (not shown here).

3.2. Stratification observed

The stratification in June 2011 at 0°N, 10°W calculated for the glider deepy during deployment no. 16 (Fig. 8 (a)) shows a diurnal pattern. Especially when considering the upper 15 m, there is weak stratification at night and maximum stratification in the afternoon. More precisely for 2 m to 6 m depth (Fig. 8 (b)), the stratification is weakest just before sunrise from 05:00 to 06:00 SAT and reaches its maximum 1-2 hours after solar noon from 13:00 to 14:00 SAT. The peak stratification of $2.2 \times 10^{-4}\ \mathrm{s^{-2}}$ is about one order of magnitude higher than values during the early morning. It propagates downward in the afternoon and early evening when convective cooling starts to reduce the stratification in the upper 6 m (Fig. 8 (a)). Below the upper 15 m, there is a stratification maximum of $5.1 \pm 0.5 \times 10^{-4}\ \mathrm{s^{-2}}$ at $25\ \mathrm{m} \pm 4\ \mathrm{m}$ depth which does not show a discernible diurnal pattern. The same is true for greater depth.

Comparing the stratification of the upper 2 m to 6 m at 0°N, 10°W in June 2011 to the equatorial transect in October 2019 (Fig. 8 (b)) yields similar diurnal patterns regarding both shape and absolute values. However, there are some differences. The main distinction is that the TSG data at $4.04\ \mathrm{m} \pm 0.38\ \mathrm{m}$ have hardly a loss in stratification in the early morning with values remaining at about $0.4 \times 10^{-4}\ \mathrm{s^{-2}}$

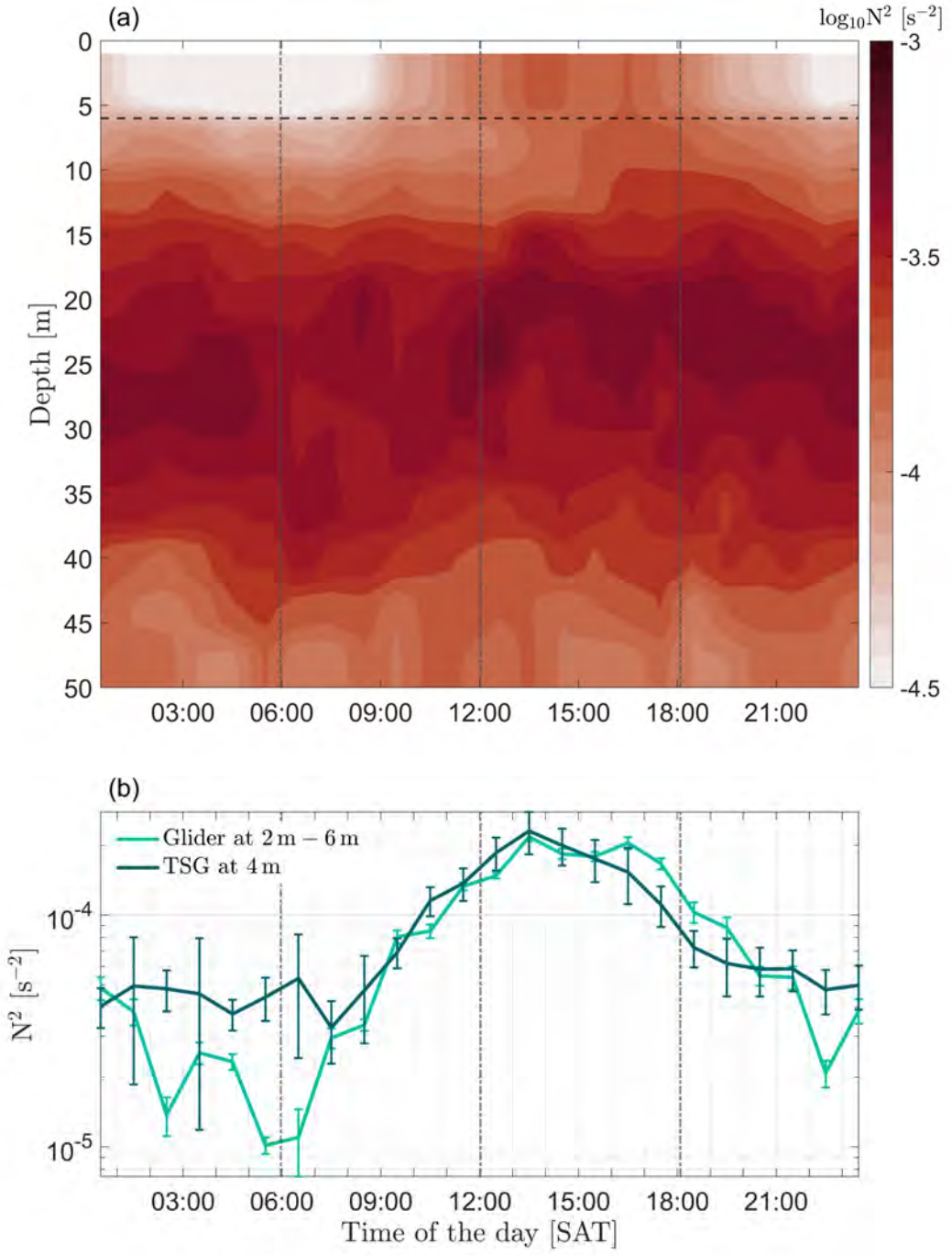

Figure 8: (a) Diurnal cycle of stratification plotted as a function of the depth and the time at 0°N, 10°W in June 2011 during deployment no. 16 of the glider deepy. (b) Diurnal cycle of stratification close to the surface. Dark green shows mean values between 2 m and 6 m for deployment no. 16 of the glider deepy. Light green is an estimate for stratification from the TSG at 4 m for the equatorial section of the TRATLEQ1 cruise. Further, the vertical grey lines mark sunrise, noon and sunset. The horizontal dashed black line in (a) denotes 6 m depth.

while the glider values drop to 0.1×10^{-4} s^{-2}. Further, for the TSG data the stratification starts to bulid up 1 hour later than for the glider with the curves aligning afterwards. While for both datasets the stratification reaches its maximum between 13:00 and 14:00 SAT, the duration of the peak differs. While for the TSG data the stratification decreases straight after the peak, the maximum stratification persists for about 3 hours in the glider data.

Influence of wind on stratification The timeseries of stratification at 4 m along the equator is characterized by low values at night and varying strength during daytime going along with changes in the wind speed. Here, daily means of wind speed and stratification are compared (Fig. 9). They show a high negative correlation (-0.7) indicating weaker stratification for higher winds. In particular, there seems to be a threshold wind speed of ~ 6 m s^{-1}. For stronger winds, stratification values remain low and only a weak DWL is formed. For weaker winds, stratification increases significantly which means that a pronounced DWL is formed. This results in a mean stratification of 0.6×10^{-4} s^{-2} above and of 1.5×10^{-4} s^{-2} below the named threshold. The mean wind speed at 10 m height of the equatorial transect during the TRATLEQ1 cruise in October 2019 amounts to 6.8 ± 2.0 m s^{-1}. For a potential comparison with the PIRATA mooring wind measurements at 4 m height, note that the mean TRATLEQ1 wind speed calculated to 4 m height is 5.7 ± 1.8 m s^{-1}.

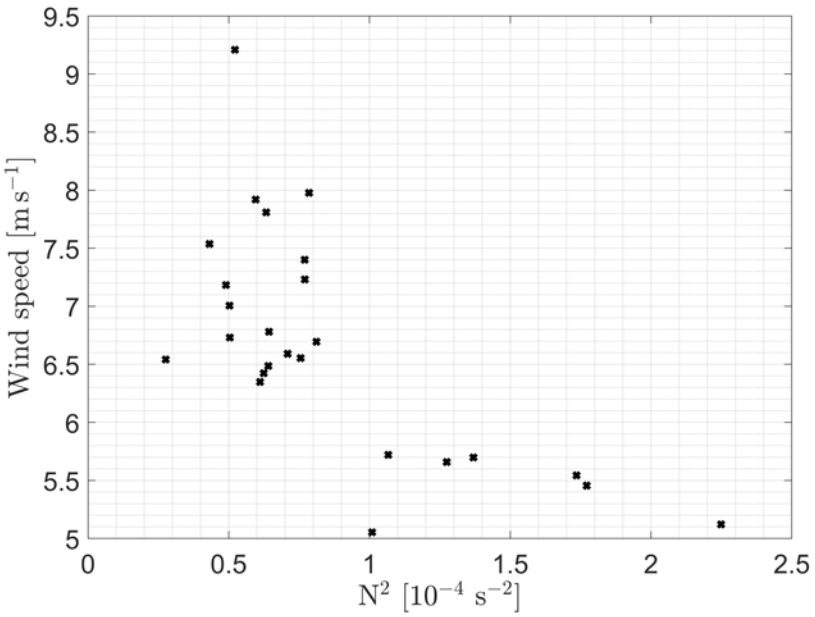

Figure 9: Daily means of stratification at 4 m depth versus wind speeds at 10 m height derived for the equatorial section in October 2019 during the TRATLEQ1 cruise.

3.3. TKE dissipation observed

The TKE dissipation rate ϵ in June 2011 at 0°N, 10°W calculated for the glider deepy during deployment no. 16 (Fig. 18 (a)) shows different diurnal patterns with depth. There is a deep diurnal cycle (deep cycle turbulence) between ~ 8 m and ~ 35 m with minimum values in the afternoon and maximum values in the morning hours ranging more than one order of magnitude. Deep cycle turbulence is described in more detail in appendix C. Below ~ 35 m, TKE dissipation is diminishing with mean values at 50 m of $3 \pm 7 \times 10^{-8}$. There is no clear diurnal pattern visible anymore at these depths. Closer to the surface, ϵ has a diurnal pattern with maximum dissipation rates around noon. This maximum is propagating downward in the afternoon and evening, contributing to the deep cycle turbulence. For 2 m to 6 m depth (Fig. 18 (b)), there is a maximum of TKE dissipation around solar noon with a peak between 12:00 and 13:00 SAT of 4×10^{-6} m^2 s^{-3}. A minimum of 4×10^{-8} m^2 s^{-3} is reached from 16:00 to 17:00 SAT. Dissipation remains low until sunrise and starts to increase between 06:00 and 07:00 SAT. This leads to a diurnal cycle of two orders of magnitude. Note that for this section data not additionally edited by hand were also considered, contrary to the following sections.

3.4. Dissipation of the WPI in the upper 6 m

The WPI provides mechanical energy for mixing which is partly dissipated by turbulence in the upper 6 m (Fig. 11). The WPI, calculated for the 0.6 m surface velocities of the CARTHE drifters during the TRATLEQ1 drifter experiment, amounts on average to $4.1 \pm 1.7 \times 10^{-6}$ m^3 s^{-3}. It shows a diurnal cycle ranging half an order of magnitude with a maximum of 7.7×10^{-6} m^3 s^{-3} between 15:00 and 16:00 SAT and a minimum of 2.5×10^{-6} m^3 s^{-3} between 00:00 and 01:00 SAT. The main increase in WPI after the minimum in the morning starts at 09:00 SAT. It should be noted that the diurnal mean of the WPI calculated for CARTHE velocities (considering the diurnal signal) is 39% higher than the one fictively calculated for SVP velocities (without the diurnal signal). This is described in more detail in appendix A. The vertically integrated TKE dissipation rate between 2 m and 6 m ($\epsilon_{\text{int2-6}}$) averages $1.3 \pm 2.1 \times 10^{-6}$ m^3 s^{-3}. There is a distinct diurnal cycle ranging two orders of magnitude. Maximum dissipation is reached between 11:00 and 12:00 SAT with 8.1×10^{-6} m^3 s^{-3} and dissipation of less than 7×10^{-7} m^3 s^{-3} is present from 15:00 to 09:00 SAT.

From 9:30 to 12:30 SAT, the maximum of $\epsilon_{\text{int2-6}}$ is of the same order as the WPI in the statistical mean. This implies that a large fraction of wind energy directly dissipates in the upper meters during early noon. For evening and morning, the WPI

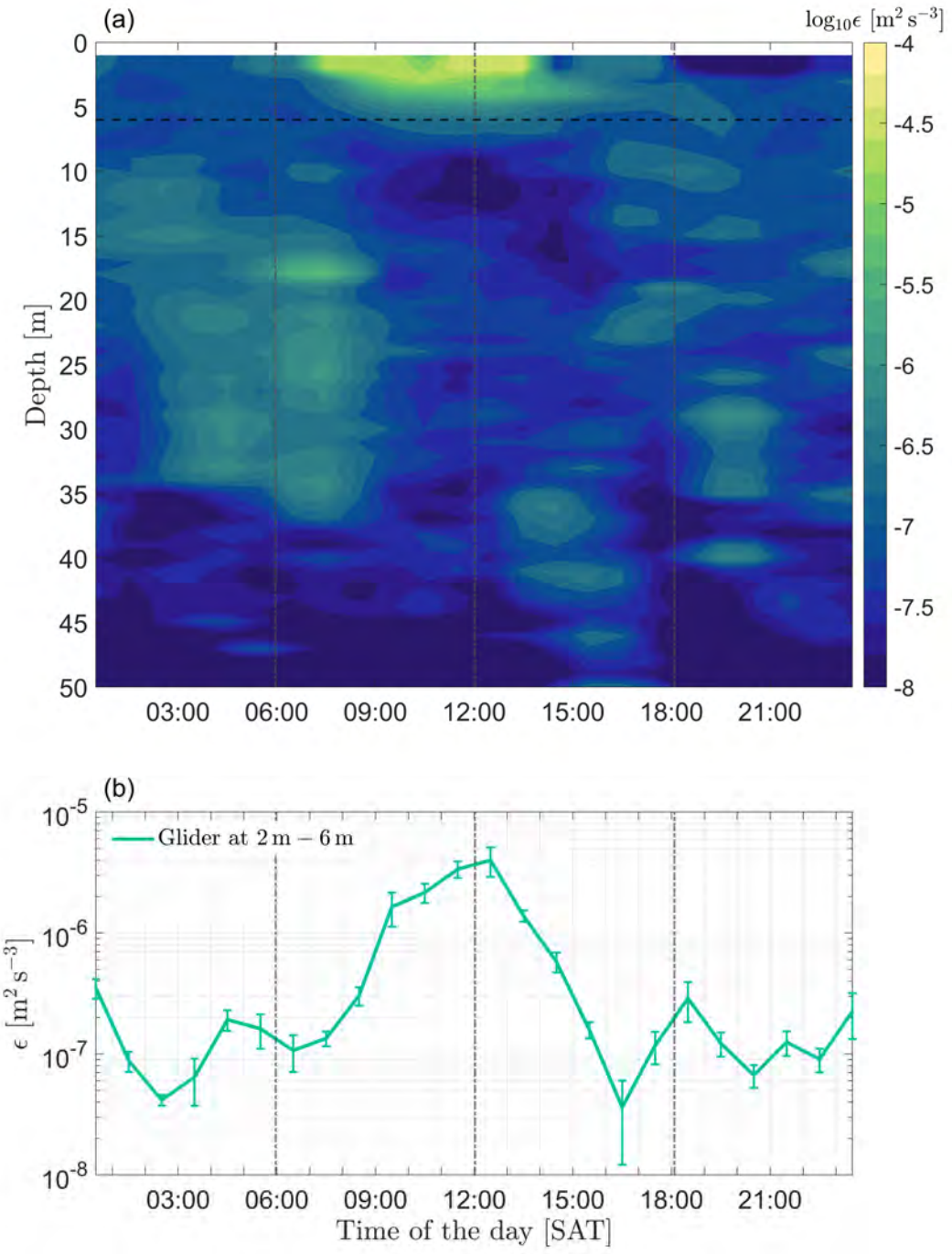

Figure 10: Diurnal cycle of ϵ (a) plotted as a function of the depth and the time and (b) as mean for $2-6$ m derived at $0°\mathrm{N}, 10°\mathrm{W}$ in June 2011 from the glider deepy during deployment no. 16. The vertical grey lines mark sunrise, noon and sunset. The horizontal dashed black line in (a) denotes 6 m depth.

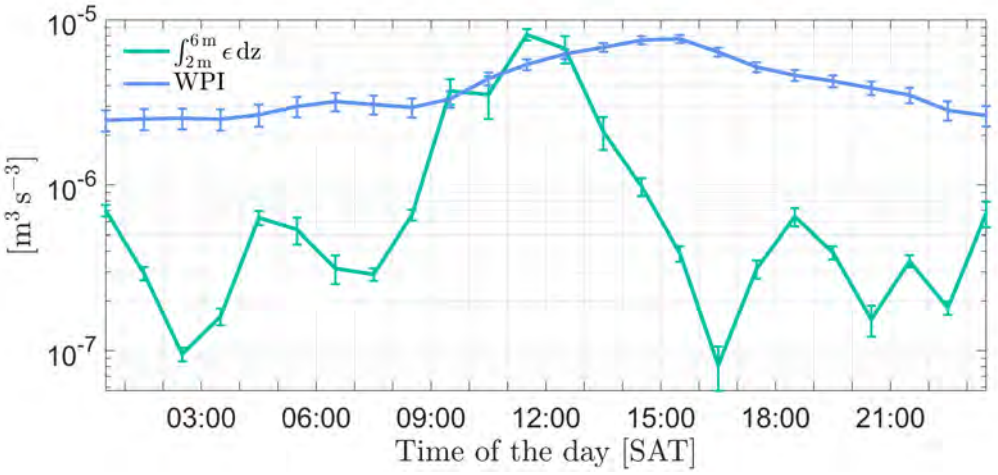

Figure 11: Diurnal cycle of (light green) the vertically integrated TKE dissipation rate between 2 m and 6 m derived at 0°N, 10°W in June 2011 from the glider deepy deployment no. 16 and of (light blue) the WPI for CARTHE drifters during the TRATLEQ1 drifter experiment in October 2019.

and $\epsilon_{\mathrm{int2-6}}$ differ about one order of magnitude. Therewith, the results reveal that the dissipation of WPI in the upper 6 m and thus the input of wind energy into the ocean differs at day and night.

3.5. Shear estimated from a mixing parameterisation

The KWB mixing parameterisation commonly estimates the mean TKE dissipation for a given shear and stratification. Here, this parameterisation is used to calculate the shear from 2 m to 6 m for the corresponding stratification and dissipation within this depth range. The diurnal cycles for stratification and dissipation obtained at 0°N, 10°W in June 2011 from the glider deepy deployment no. 16 have been described in section 3.2 and 3.3, respectively. It can be noted again that both parameters peak at different times of the day (Fig. 12). The TKE dissipation is at its maximum between 12:00 and 13:00 SAT and drops rapidly one hour later. Stratification reaches its maximum between 13:00 and 14:00 SAT with high values persisting for about 3-4 hours. The shear resulting from the KWB parameterisation (Fig. 12) is dominated by a diurnal cycle with minimum values of about 0.01 s^{-1} in the early morning and a maximum of 0.036 s^{-1} between 11:00 and 13:00 SAT. The increase in shear starting at 07:00 SAT happens faster than the decrease after the noon maxima. The 95% CI shows a wider range between 09:00 and 13:00 SAT compared to the rest of the day, which is accompanied by higher standard errors of TKE dissipation at that time. Moreover, the KWB shear estimation between 2 m and 6 m shows a different diurnal cycle compared to the shear between 1 m to 15 m calculated for the TRATLEQ1 drifter experiment in October 2019 which

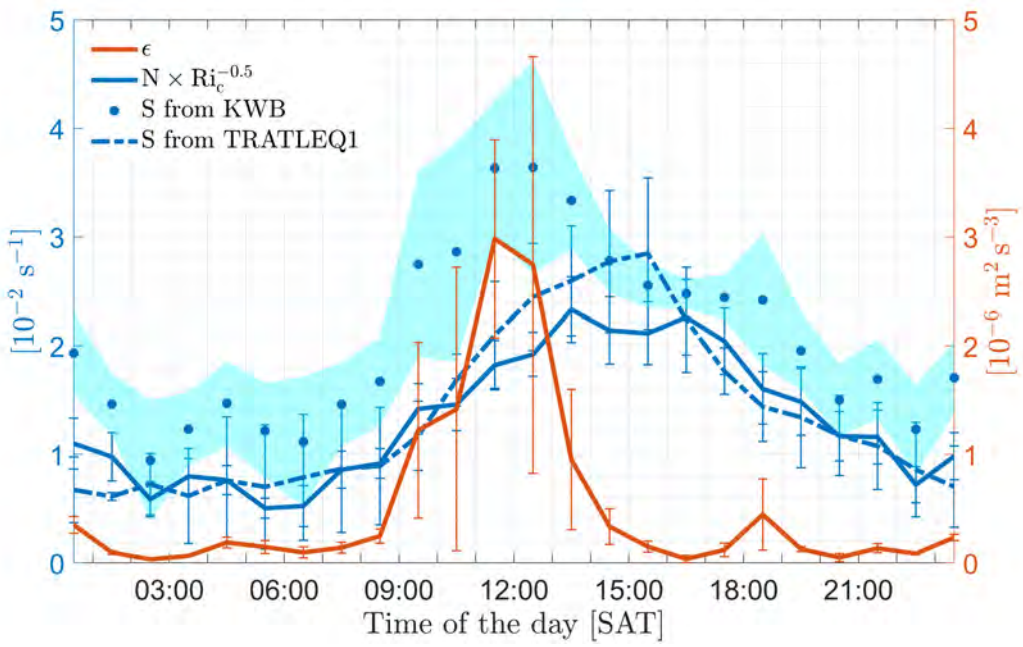

Figure 12: Diurnal cycle of (red) mean ϵ and (blue solid) mean $N \times Ri_c^{-0.5}$ between 2 m and 6 m derived at 0°N, 10°W in June 2011 from the glider deepy. The factor $Ri_c^{-0.5}$ is chosen, such that the shear and stratification curves equal for $Ri = Ri_c$. The shear resulting from the KWB mixing parameterisation is denoted with blue dots. The light blue area marks the 95% confidence interval obtained by bootstrapping. For comparison (blue dashed), the diurnal cycle of shear during the TRATLEQ1 drifter experiment in October 2019 is shown, assuming that shear is linearly distributed between 2 m and 6 m and zero below.

has been described in section 3.1. The maximum shear occurs 3.5 hours earlier for the KWB estimate. Moreover, the resulting shear values are always (except from 15:00 to 16:00 SAT) higher than the observed shear between 1 m and 15 m depth, even if assuming that the latter is linearly distributed between 2 m and 6 m and that it vanishes below. In numbers, the KWB shear maximum is 28% higher than the adapted 2 m to 6 m TRATLEQ1 shear maxima. For 23:00 to 02:00 SAT and 09:00 to 10:00 SAT, KWB shear exceeds the adapted TRATLEQ1 shear values by more than 100%. Still, the orders of magnitude are comparable. Contrasting the absolute values, it should be noted that the KWB shear values need to be higher than stratification values multiplied by $Ric^{-0.5}$ in order to have dissipation present according to the setup of the parameterisation.

4. Discussion and Conclusion

This study focused on the diurnal behaviour of shear, stratification and TKE dissipation in the upper equatorial Atlantic as well as on the role of the wind speed in this regard. The respective parameters were analysed using observational data obtained from the TRATLEQ1 cruise, a glider mission, Argo floats and CARTHE as well as SVP surface drifters in the equatorial Atlantic. These datasets indicate a stronger diurnal amplitude of the named parameters in the top 2 m to 6 m than at 10 m depth and below. Further, it was shown that the near-surface diurnal cycle influences the dissipation of wind energy as well as contributes to the deep diurnal cycle.

Near-surface shear Due to a lack of velocity measurements in the upper 2 m to 6 m of the ocean, observations at 1 m and 15 m depth were considered for this study. The TRATLEQ1 drifter experiment and cruise data revealed that the shear between 1 m and 15 m currents is mainly present in the along wind component and hardly in the across wind component. Consequently, the near-surface shear in the equatorial Atlantic in October 2019 was primarily wind-driven, corresponding with the occurrence of a diurnal jet described in various earlier studies (e.g. Smyth et al., 2013; Hughes et al., 2020; Masich et al., 2021).
The TRATLEQ1 cruise and drifter datasets yield a similar distinct diurnal cycle peaking between 14:00 and 16:00 SAT and minimising between 05:00 and 06:00 SAT. However, a different behaviour in the morning results in a 22% smaller diurnal amplitude for the shear between Radar and vmADCP velocities compared to the shear between CARTHE and SVP velocities. While the shear vanishes for the latter in the early morning, the former still shows a background shear. This background shear corresponds roughly to northward shear with the wind being mainly directed northward in October 2019. Hence, the background shear could be the result of the equatorial roll which acts directly at the equator (Heukamp et al., 2022) yielding northward shear linearly depending on the meridional wind stress. This effect is apparent for the Radar and vmADCP measurements (limited to the region between 0.01°S and 0.01°N) but the CARTHE and SVP measurements (limited to the region between 1°S and 1°N) are already too far from the equator to see this effect. Therewith, the equatorial roll can explain the nighttime differences in shear values but not the larger diurnal amplitude obtained by the drifter measurements compared to the shipboard measurements. The wind slip is also no possible explanation for the differences in amplitude as SVP drifters are supposed to be more affected by wind drift than CARTHE drifters (Poulain et al., 2022) which would imply a smaller instead of a larger amplitude. Remaining possible explanations are the varying penetration

depth of the Radar as well as temporal and spatial differences in sampling. Nonetheless, the diurnal cycles of the TRATLEQ1 datasets match well with their diurnal amplitudes ranging between 0.090 $\mathrm{m\,s^{-1}}$ and 0.115 $\mathrm{m\,s^{-1}}$. These amplitudes are in line with results from Wenegrat and McPhaden (2015) for shear between 3.75 m and 20 m depth in the equatorial Atlantic as well as results from Masich et al. (2021) at 10 m depth in the eastern equatorial Pacific.

The relevance of this diurnal cycle between 1 m and 15 m velocities is stressed by its influence on the WPI. The WPI and thus the possible energy for mixing increases in the diurnal average by 39% considering the diurnal cycle in 1 m depth instead of taking the 15 m velocities without the diurnal signal. However, some studies still use SVP velocities as surface values (e.g. Yu et al., 2019) and thus underestimate the available surface kinetic energy.

In addition to the observations of the 1 m and 15 m currents, the KWB mixing parameterisation provides an estimate for the mean shear between 2 m and 6 m depth. This gives not only an idea of the vertical distribution of shear but also makes shear comparable with the stratification and TKE dissipation observed close to the surface. The parameterisation produces a diurnal cycle for shear with a 3.5 hours earlier and 28% stronger diurnal peak as well as a larger diurnal amplitude than the shear obtained from the 1 m and 15 m velocity measurements. Trusting the applicability of the parameterisation, this implies an evolution of the diurnal jet with maximum shear propagating downward with time. For the comparison of absolute values it should be noted that the magnitude of the shear estimate depends on the value of $\mathrm{Ri_c}$. In this study only the vertical derivative scale and not the ratio of the shear variance to the mean stratification were considered for choosing the appropriate $\mathrm{Ri_c}$ due to a lack of fitting shear data. This is a possible error source. However, the higher shear values from 2 m to 6 m depth compared to 1 m to 15 m depth might be the result of the shear being concentrated closer to the surface during the buildup of the DWL. While previous research by Smyth et al. (2013) has focused on processes below 10 m depth showing a strengthening along the descending shear layer, this study suggests a different behaviour in the upper 10 m. This implies a minimum of the diurnal jet amplitude at roughly 10 m depth. Furthermore, the timing of the diurnal peak between 1 m and 15 m presented in this study is in agreement with Wenegrat and McPhaden (2015). Yet, Smyth et al. (2013) calculated a diurnal peak for shear at 15 m depth at 15:00 LT and therefore at the same point in time we obtained a diurnal peak for the mean shear between 1 m and 15 m depth. Considering the buildup and descent of the shear layer following from Smyth et al. (2013) as well as the KWB shear estimate, there would need to be a time lag. It is beyond the

scope of this study to explain the discrepancy in timing. Higher vertically resolved velocity data in the upper meters of the ocean are necessary to better understand the vertical distribution of shear as well as to verify the suggested patterns of the shear between 2 m and 6 m depth.

The shear between 1 m and 15 m depth obtained from Argo surface and SVP velocities during the period 2000 to 2020 is validated to allow a larger spatial and temporal coverage compared to the TRATLEQ1 datasets. It is shown that the herein before mentioned diurnal cycle between 1 m and 15 m currents can be represented regarding shape and magnitude. Yet, the resulting diurnal cycles for both all calendar months as well as boreal autumn months only (coinciding with the TRATLEQ1 period) are smoothed and go along with large uncertainties. This may result from: (1) the Argo surface time which can amount up to 6 h in this study; (2) the weak spatial and temporal resolution of the Argo surface velocities. Both factors have an impact on the reliability of the emerging shear whose analysis should be treated with care accordingly. However, note that with the present Argo surface time of about 2 hours remaining in the future, the picture could get clearer in the next years. Nonetheless, few datapoints and coarse spatial and temporal resolution will remain an issue. Hence, the shear data derived from Argo surface values can only be used to derive a general pattern but not to get accurate values.

Near-surface stratification The stratification close to the surface also follows a diurnal cycle with the diurnal maximum from 13:00 to 14:00 SAT for both the measurements at $0°\mathrm{N}, 10°\mathrm{W}$ in June 2011 and for the equatorial transect in October 2019. The main difference in the diurnal cycle for glider and TSG measurements at about 4 m is a decrease of stratification until sunrise for glider measurements while TSG values remained approximately constant during the early morning. The resulting difference in the diurnal amplitude might be a consequence of differences in sampling as well as of regional, seasonal and interannual variability. The amplitude of the diurnal cycle decreases with depth. Besides, the occurrence of the diurnal maximum is consistent with the findings of Wenegrat and McPhaden (2015), who found a temperature maximum at 1 m depth at 14:00 LT. Likewise, the simulation for an idealized DWL by Hughes et al. (2020) also yields a temperature and stratification maximum at 14:00 LT. However, the timing does not match the outcome by Smyth et al. (2013) who proposed an earlier stratification maximum. One possible explanation is spatial and temporal variability of the decent rate for the DWL and the diurnal jet. No differences in the diurnal cycle of stratification at the surface can be expected as it mainly depends on the diurnal cycle of solar radiation.

Near-surface TKE dissipation The diurnal TKE dissipation rate in the top 2 m to 6 m reaches its maximum between 11:00 and 12:00 SAT, as glider data at 0°N, 10°W in June 2011 showed. Values in the evening and morning are about two orders of magnitude lower. With that, the amplitude of the diurnal cycle at the surface is about one order of magnitude larger than the amplitude of deep cycle turbulence. The presented maximum TKE dissipation of 3×10^{-6} $\mathrm{m^2\,s^{-3}}$ between 2 m to 6 m fits in with the order of maximum deep cycle turbulence obtained at 10 m depth at 0°N, 140°W by Smyth et al. (2013). Yet, our measurements exceed the maxima of deep cycle turbulence at 21 m depth as well as ML measurements in the equatorial Atlantic by one order of magnitude (Moum et al., 2022; Hummels et al., 2014). Having in mind that deep cycle turbulence is stronger in the equatorial Pacific than in the equatorial Atlantic (Moum et al., 2022), our results match earlier studies if the diurnal peak is about one order of magnitude increased at 2 m to 6 m depth range compared to the deep cycle below 20 m.

The relevance of this diurnal maximum is stressed by comparing $\epsilon_{\mathrm{int2-6}}$ with the WPI obtained from CARTHE velocities of the TRATLEQ1 drifter experiment. It should be noted that in some cases (e.g. for passing TIWs) the 1 m current velocity can be reversed to the wind velocity which leads to a negative WPI decelerating the 1 m current. Although in this case the kinetic energy of the mean current is reduced, shear and dissipation can still be created. Hence, $\epsilon_{\mathrm{int2-6}}$ equalling the WPI in the diurnal mean does not necessarily imply that the WPI is entirely dissipated. The average WPI amounts to $52.8 \pm 4.1 \times 10^{-7}$ $\mathrm{m^3\,s^{-3}}$ which is equivalent to $5.28 \pm 0.41 \times 10^{-3}$ $\mathrm{W\,m^2}$. This value is in line with near-equatorial WPI estimates from Flexas et al. (2019) for the time mean motion as well as from Rimac et al. (2016) for both the time mean motion and near-inertial motions. Although seasonal and intraseasonal WPI variability are possible, the orders of magnitude should still be comparable between June 2011 and October 2019, especially since climatological wind speeds in June and October are similar (Wenegrat and McPhaden, 2015). In the statistical mean, $\epsilon_{\mathrm{int2-6}}$ is of the order of the WPI from 9:30 to 12:30 SAT and about two orders of magnitude smaller during night. This implies that a large fraction of wind energy is directly dissipated in the upper meters during early noon, coinciding with the time of increasing stratification. Therefore, the contrasting diurnal behaviour should be taken into account when considering how to parameterise turbulence and the dissipation of wind energy in the upper 2 m to 6 m.

All in all, this study pointed out the diurnal cycle in the upper 2 m to 6 m of the ocean for shear, stratification and TKE dissipation. The diurnal amplitudes are

decreasing with depth yielding a difference of up to 1 order of magnitude comparing the near-surface and the deep diurnal cycle. After sunrise near-surface stratification and shear start to increase. While the DWL and the diurnal jet are building up, there is pronounced TKE dissipation. The latter drops once the near-surface shear starts decreasing and thus once Ri starts increasing. Following from that, there seems to be no time lag between the shear-instabilities and turbulence. Former studies suggested a time lag of 2-3 hours (Smyth et al., 2013). The near-surface stratification maximum persists longer and lags shear and TKE dissipation by about 2 hours. Further, the near-surface diurnal cycle sets in several hours earlier than the deep diurnal cycle.

Influence of wind Moreover, the datasets indicate that the shear and the stratification and hence the formation of the DWL as well as the diurnal jet are influenced by the wind speed. TRATLEQ1 data reveal a negative correlation between stratification at about 4 m depth and the wind speed with a threshold of $\sim 6\ \mathrm{m\,s^{-1}}$. A pronounced diurnal warm layer forms for wind speeds below. For shear, no direct relationship to the wind speed is found, contradicting the claims of Masich et al. (2021) that the wind speed linearly relates to the diurnal amplitude of velocity. However, it is shown that the diurnal pattern varies for different wind speeds. While the wind momentum is too little to generate a diurnal jet for low wind speeds ($0 - 3\ \mathrm{m\,s^{-1}}$), there is a diurnal jet for moderate ($4 - 6\ \mathrm{m\,s^{-1}}$) and high ($8 - 12\ \mathrm{m\,s^{-1}}$) winds. For high wind speeds, the amplitude of the diurnal shear cycle increases and the peak narrows, suggesting a strong though shorter persisting diurnal jet, compared to moderate wind conditions. The latter might be caused by a weak DWL. Another explanation is an increase of the penetration depth of the diurnal jet with higher wind speeds (Masich et al., 2021). This would also yield a diurnal jet being visible for a shorter period in the upper 15 m of the ocean. These wind dependencies go along with the simulation from Hughes et al. (2021) considering similar wind groups. Albeit, they suggested no DWL for strong winds which is not the case here as a DWL (even a weak one) is needed to explain the diurnal pattern for shear. Further, it should be noted that the wind slip for drifter and hence most probable also for the Argo surface drift measurements depends on the wind speed (Novelli et al., 2017) though no studies about the quantification of the wind drift of Argo floats at the surface are known. Nevertheless, it is assumed that the uncertainty of the shear derived from Argo surface and SVP values exceeds the possible wind slip, whereby the latter is not considered further in the analysis.

Seasonality Winds at the equator follow seasonal patterns due to the meridional migration of the ITCZ and therefore induce seasonal patterns for shear and stratification. This analysis indicates a distinct diurnal cycle of shear velocities between 1 m and 15 m depth and hence a distinct diurnal jet in the months with strongest mean wind speeds (July to October). In the months with weaker mean wind speeds (January to May), the formation of the diurnal jet is hardly visible. This concurrence of months with strong trade winds and a pronounced diurnal jet and vice versa confirms the findings of Wenegrat and McPhaden (2015) who analysed an 8 months period.

Further, Wenegrat and McPhaden (2015) showed seasonal variations for the diurnal SST amplitude yielding a marked DWL in January to May and a weaker DWL in June to December. Considering monthly wind averages, these results go along with the earlier proposed threshold of $\sim 6\ \mathrm{m\,s^{-1}}$ for the presence of a pronounced DWL. Following the KWB parameterisation, there is a relation between shear, stratification and dissipation. Therefore, it can be expected that likewise the TKE dissipation rate is influenced by wind speed and follows seasonal patterns. Earlier studies revealed the seasonality of deep cycle turbulence (Wenegrat and McPhaden, 2015; Smyth et al., 2021), being caused by changes in the trade winds with a particular spring minimum. However, the near-surface diurnal cycle of TKE dissipation does not necessarily need to show the same seasonal pattern as the deep diurnal cycle. On the one hand, instabilities that trigger turbulence propagate downwards linking the existence of turbulence in the two depth ranges. On the other hand, the strength of deep cycle turbulence depends on the presence of marginal instability above the EUC which does not play a role at the near-surface anymore. For the beginning of the year (January to May), it can be expected that with weaker shear between 1 m and 15 m depth but a pronounced DWL in comparison to the remaining year, there will be an increase in Ri reducing the likelihood of shear-instabilities and hence TKE dissipation to occur. Vice versa, for July to October a stronger diurnal jet and a weaker DWL might decrease Ri raising the likelihood of shear-instabilities to occur. To compute the seasonality of near-surface TKE dissipation and thus to verify these expectations, there is a need for either more near-surface data for the TKE dissipation or a reliable estimate for near-surface shear. The latter aspect repeats the importance of higher vertically resolved shear data close to the surface.

While previous research has mainly focused on diurnal processes below 10 m depth, this study demonstrates that processes in the upper 10 m should be taken into account for calculating and parameterising the near-surface heat and momentum

budgets. In particular, the respective processes can be important for understanding the vertical distribution of shear, and with that, they can improve turbulence parameterisations. The near-surface processes also impact air-sea fluxes, especially regarding the dissipation of WPI. Although several different datasets were analysed, there are still open questions regarding the vertical distribution of horizontal shear close to the surface. Besides, most observational data used in this study were taken during strong and steady trade winds. More observations during the season with weaker winds can help to verify the conclusions made for the dependence of shear and stratification on the wind.

A. TRATLEQ1 drifter experiment

During the TRATLEQ1 cruise (M158), drifters were deployed to intensely monitor shear between 1 m and 15 m currents in the equatorial Atlantic. Therefore, 27 CARTHE drifters (following 0.6 m $\approx$ 1 m currents) and 31 SVP drifters (following 15 m currents) were deployed. The CARTHE drifters are 85% biodegradable and include a donut-shaped top component, carrying the GPS and batteries, attached to a rigid cross-shaped drogue (Novelli et al., 2017). They present minimal wave rectification issues and their wind-induced slip velocity is less than 0.5% of the neutral wind speed at 10 m height. However, in the presence of large waves, the error of the CARTHE velocities can increase to a few $\mathrm{cm\,s^{-1}}$ (Poulain et al., 2022). The absolute slip velocity during laboratory testing was found to decrease with increasing wind speed, likely caused by wind separation from the ocean surface due to the presence of surface gravity waves (Novelli et al., 2017). Comparing the slip for CARTHE and SVP drifters, it should be noted that SVPs have more direct wind drag above the sea surface compared to CARTHE drifters (Poulain et al., 2022).

The SVP drifters consisted of 5 GDP SVP-B (with additional pressure sensor), 11 GDP SVP, 5 E-SURFMAR SVP-B (with additional pressure sensor), 5 Copernicus SVP-BRST (with additional pressure sensor) and 5 SIO DWS-D (with additional sensors for pressure and directional properties of waves). The spatial resolution is $0.0001° = 0.01$ km for CARTHE and Copernicus BRST, $0.0003° = 0.03$ km for SIO DWS-D and $0.001° = 0.1$ km for the remaining SVP drifters. The temporal resolution is irregular for CARTHE and mostly hourly for SVP drifters. Therefore, the original data were linearly interpolated to an hourly grid for values less than 4 h apart. Further, the quality of data was validated to account for GPS errors and other failures. The following criteria were taken into account: 1. The status of the drogue had to be on. 2. A maximum velocity criterion of $3\ \mathrm{m\,s^{-1}} \approx 10.8\ \mathrm{km\,h^{-1}}$ was applied (compare Lumpkin and Pazos (2007)). 3. A maximum acceleration criterion of $1\ \mathrm{km\,h^{-2}}$ was

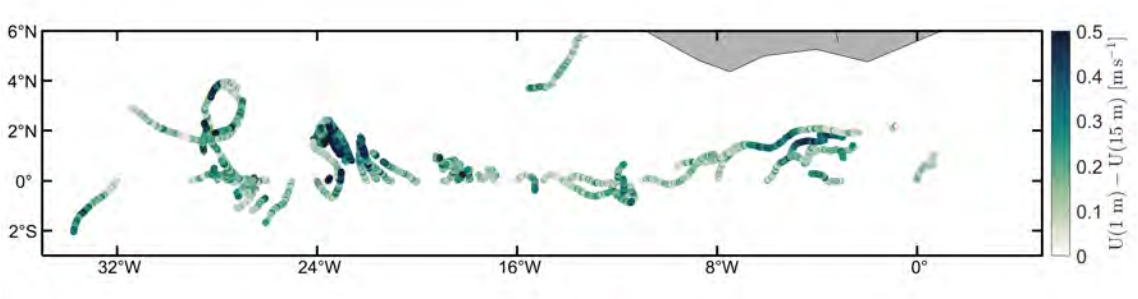

Figure 13: Position of collocated CARTHE and SVP drifters from the TRATLEQ1 drifter experiment with the resulting absolute shear velocity in color.

used. 4. Drifters with constant velocities for more than 5 h were removed as they are considered grounded. 5. Drifters fetched by ships were removed manually. Note that for the CARTHE drifters a drogue loss still cannot be excluded which would result in higher velocities (Lodise et al., 2019). Yet, a drogue loss is unlikely as there have not been large storm and wave events during the deployment (Haza et al., 2018).

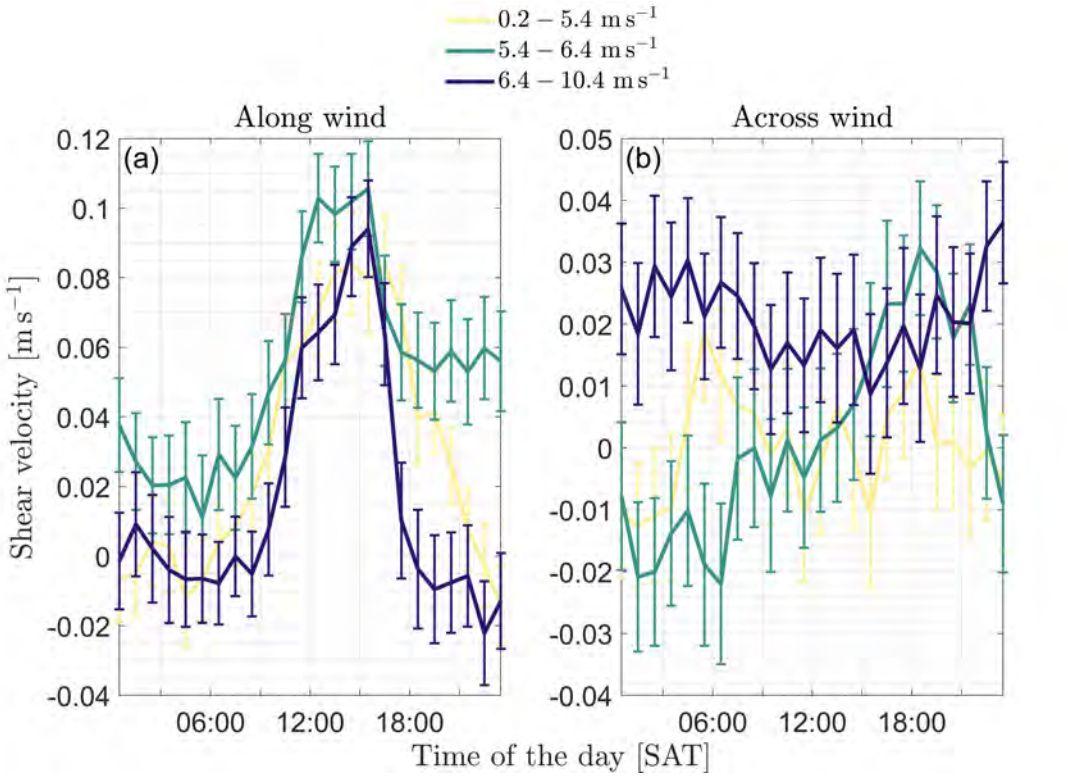

Figure 14: Diurnal cycle of shear velocities in (a) the along and (b) the across wind direction for different wind speeds derived from the TRATLEQ1 drifter experiment. The three wind groups are chosen such that there is a comparable number of values in each group.

The validated and gridded trajectories for SVP and CARTHE drifers were then collocated using a maximum distance criterion of 100 km (which is about 1° in longitudinal direction) and a temporal criterion of 1 hour. Following from that, 12,408 pairs were considered from October 01, 2019 to November 28, 2019. However, 91% of the values were obtained in October. The position of the collocated values is depicted in Fig. 13. No further criterion is used to eliminate possible outliers, as a criterion of 3 standard deviations off the median removes unproportionally more values in the afternoon where shear is strongest. Hence, this criterion removes „true“ shear velocity peaks and yields a bias. For better comparison with shipboard observations, only values between 1°S and 1°N are considered in the following. The standard error was computed as $std \times f^{-0.5}$ where for the degrees of freedom f one independent value per day is assumed.

In the following, the diurnal behaviour of the described TRATLEQ1 drifter dataset is examined and contrasted to the results depicted in section 3.1. The diurnal patterns for shear velocities in the along and the across wind direction are shown in Fig. 5 and are described in section 3.1. The shape of the diurnal cycle in the along wind shear component is influenced by the wind speed (Fig. 14 (a)). For high wind speeds (here $6.4 - 10.4\ \mathrm{m\,s^{-1}}$) compared to moderate winds (here $5.4 - 6.4\ \mathrm{m\,s^{-1}}$), the afternoon peak in the along wind component is narrower and the amplitude of the diurnal cycle is larger due to vanishing shear in the evening and early morning. This indicates that the diurnal jet and likely the DWL persist shorter for higher winds. Further, the results point to well mixed upper 15 m of the ocean in these conditions. For lower wind speeds (here $0.2 - 5.4\ \mathrm{m\,s^{-1}}$) compared to moderate winds, the diurnal peak is broader and the diurnal amplitude is similar. Besides, the shear for low wind conditions vanishes in the early morning which is not the case for moderate winds, leading to highest shear values and thus the strongest diurnal jet in the moderate wind group. From the width of the peak it can be followed that the diurnal jet and likely the DWL persists longer for lower winds. Moreover, there is no clear pattern visible in the across wind shear component (Fig. 14 (b)). These results go along with the findings acquired by shear data of Argo surface and SVP velocities for moderate and high winds (Fig. 7). However, the results for low wind speeds cannot be compared for mismatching choice of wind regimes.

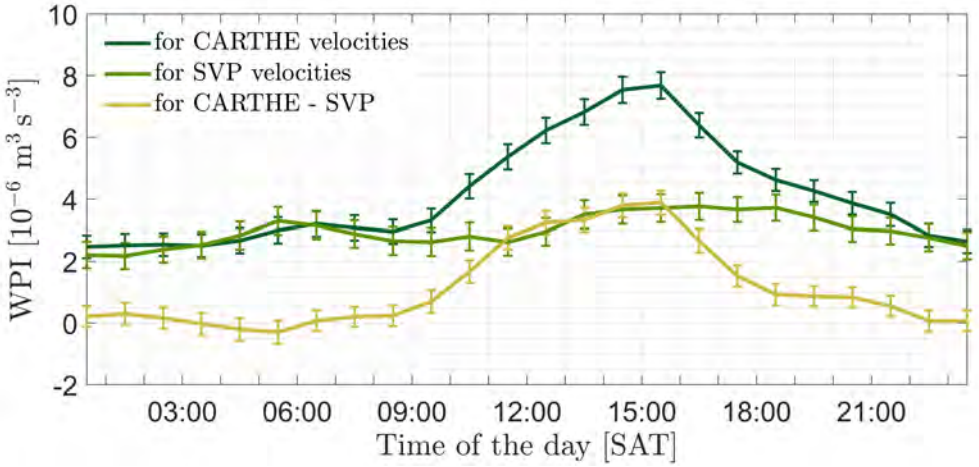

Figure 15: Diurnal cycle of the WPI derived from the TRATLEQ1 drifter experiment, assuming CARTHE (dark green), SVP (light green) and CARTHE-SVP (yellow) measurements as surface velocities.

Furthermore, the WPI is derived for CARTHE velocities. A fictive WPI is also calculated taking SVP velocities at 15 m depth as well as the shear between CARTHE and SVP velocities as surface velocities (Fig. 15). While WPI values are comparable

during night and morning hours for CARTHE and SVP velocities, there is an increase in WPI during daytime considering CARTHE velocities but an almost constant WPI considering SVP velocities. Following from that, the WPI and thus the possible energy for mixing increases in the diurnal average by 39% allowing for the diurnal cycle in 1 m depth instead of taking the 15 m velocities without the diurnal signal.

B. Deep cycle turbulence

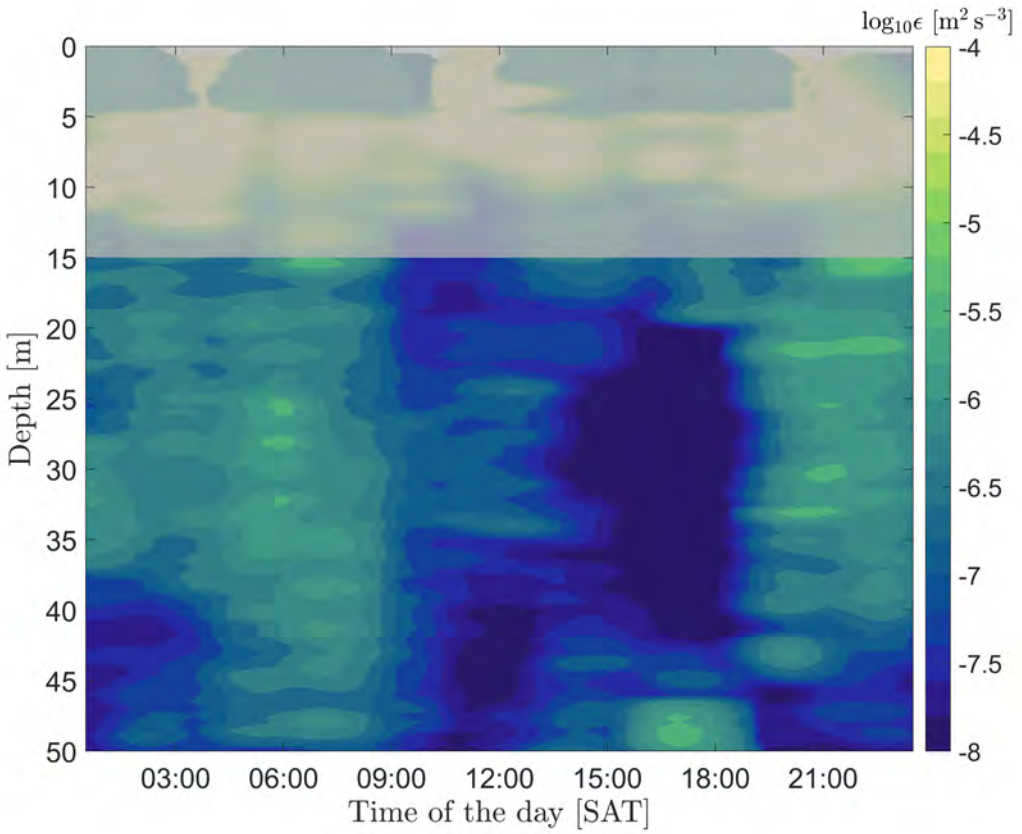

Figure 16: Diurnal cycle of ϵ plotted as a function of the depth and the time obtained along the equator during the TRATLEQ1 cruise. The grey shaded area marks data possibly influenced by ship induced turbulence.

Deep cycle turbulence is a term for the diurnal cycle of turbulence beneath a well-mixed nighttime surface layer (Moum et al., 2022). In the equatorial Atlantic and Pacific, time-mean values of TKE dissipation at the base of the ML, at nominally 30 m depth, are nearly identical (Moum et al., 2022). Comparing sites for the equatorial Atlantic, the deep diurnal cycle is stronger at 0°N, 23°W than at 0°N, 10°W going along with the EUC leveling out from 0°N, 23°W to 0°N, 10°W, from seasonal mean core depth of 73 m to 61 m. The metric of instability, defined as the fraction of hourly values that are less than $\mathrm{Ri_c} = 0.25$ at 20 m is 75% for 0°N, 23°W and 50% for 0°N, 10°W indicating that the most frequently occurring depth of $\mathrm{Ri} < \mathrm{Ri_c}$ is presumably shallower at 0°N, 10°W (Moum et al., 2022). Contrary, the deep cycle turbulence in the Pacific is more pronounced in the central and eastern basin than in the western basin likely due to the marginally unstable background flow in the central and eastern equatorial Pacific, where a shallow SEC to EUC transition results in high background shear destabilizing the fluid (Masich et al., 2021).

Microstrucure data from the TRATLEQ1 cruise are able to represent the mean deep cycle turbulence along the equatorial Atlantic (Fig. 16). For 20 m to 25 m depth, the TKE dissipation reaches its minimum between 15:00 and 18:00 SAT. A maximum of 10^{-6} $\mathrm{m^2\,s^{-3}}$ is reached in the late evening yielding a diurnal amplitude of nearly three orders of magnitude. Therewith, the deep diurnal cycle is stronger in the TRATLEQ1 data compared to the data from the glider deepy (compare Fig. 18 (a)). Furthermore, the deep diurnal cycle reaches deeper for the TRATLEQ1 data with at least 45 m compared to about 35 m for the glider deepy. A possible explanation for these differences is a weaker deep cycle at $0°\mathrm{N}, 10°\mathrm{W}$ than at $0°\mathrm{N}, 23°\mathrm{W}$ (Moum et al., 2022). This could mean that the deep cycle gets stronger towards the center of the basin and possibly also further west. Therefore, an equatorial transect encounters a stronger deep cycle than measurements at $0°\mathrm{N}, 10°\mathrm{W}$ only. Unfortunately, the turbulence data obtained during the TRATLEQ1 cruise are too sparse to analyse the longitudinal dependence. Nonetheless, the TRATLEQ1 data reveal a stronger diurnal cycle compared to a 6 year mean of Xpod measurements at $0°\mathrm{N}, 10°\mathrm{W}$ and $0°\mathrm{N}, 23°\mathrm{W}$ presented by Moum et al. (2022). The different diurnal amplitudes are in some measure the result of seasonal variations smoothing the 6 year Xpod mean. Moreover, the mean value of the TKE dissipation rate between 20 m and 50 m depth amounts to 5.2×10^{-7} $\mathrm{m^2\,s^{-3}}$ during the TRATLEQ1 cruise. This value is of the same order as the estimate for the mean TKE dissipation between 20 m and 50 m depth in October 2008 at $0°\mathrm{N}, 23°\mathrm{W}$ by Wenegrat and McPhaden (2015), assuming $\mathrm{Ri_c} = 0.25$ or $\mathrm{Ri_c} = 0.40$.

C. Equatorial section of the TRATLEQ1 cruise

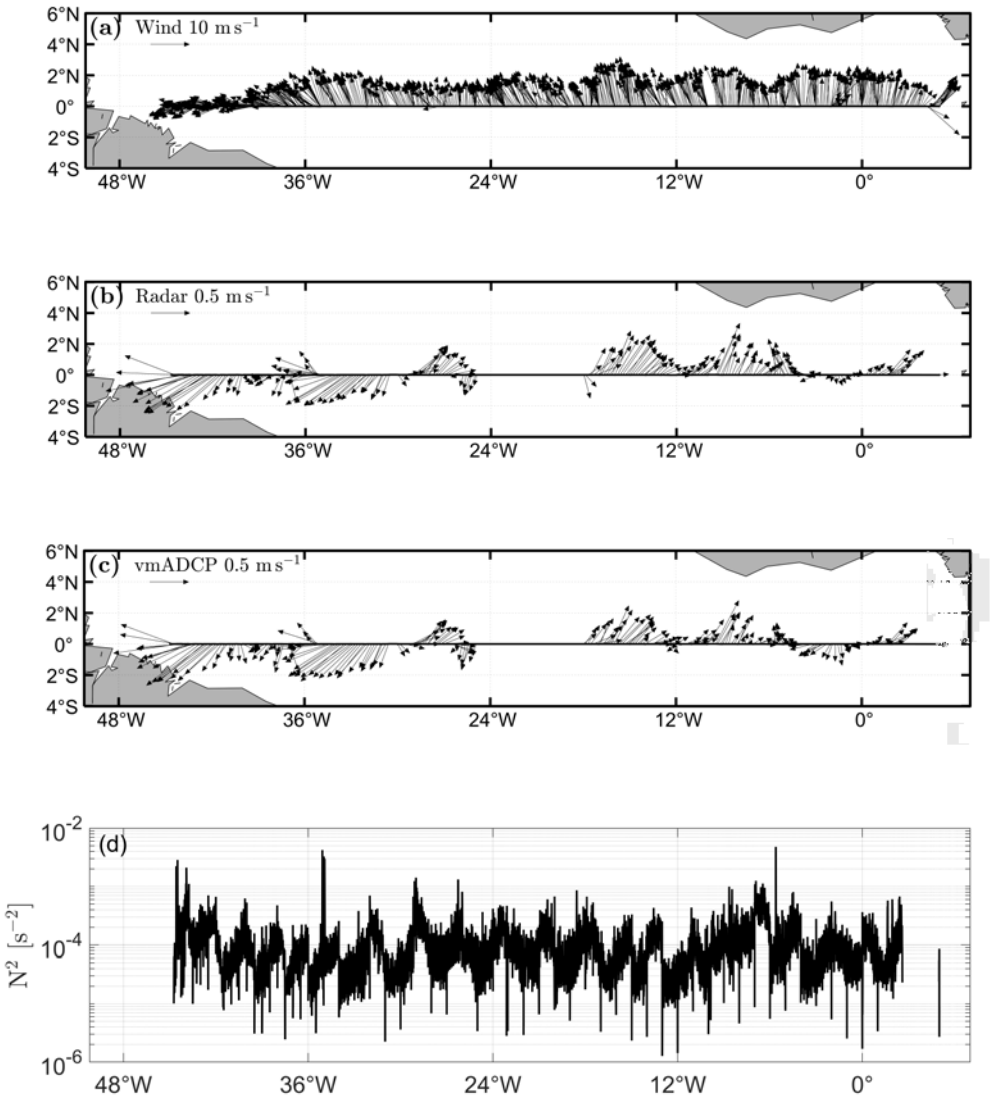

Figure 17: Equatorial section of (a) wind velocities at 30 m height, (b) Radar velocities at $\sim$ 1 m depth, (c) vmADCP velocities at 17 m depth and (d) stratification at 4 m depth. (a) presents 30 min averages, (b+c) 20 km averages. All data were obtained during the TRATLEQ1 cruise in October 2019.

D. Time series for the glider deepy

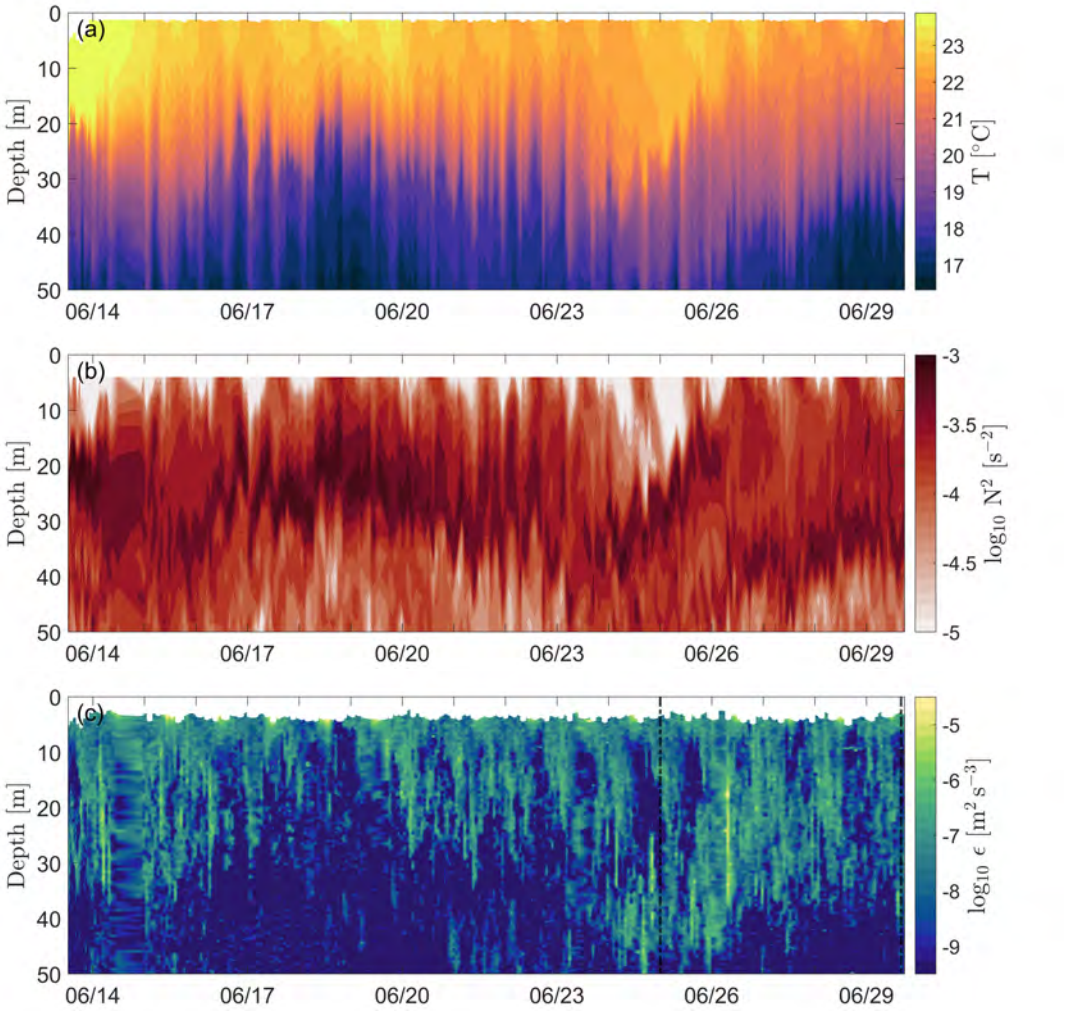

Figure 18: Time series of (a) temperature, (b) stratification and (c) ϵ plotted as a function of the depth and derived at $0°\mathrm{N}, 10°\mathrm{W}$ in June 2011 from the glider deepy during deployment no. 16. The vertical black line in (c) denotes data that were additionally edited by hand.

References

Brandt, P., Funk, A., Tantet, A., Johns, W. E., and Fischer, J. (2014). The Equatorial Undercurrent in the central Atlantic and its relation to tropical Atlantic variability. *Climate Dynamics*, 43(11):2985–2997.

Deppenmeier, A.-L., Haarsma, R. J., LeSager, P., and Hazeleger, W. (2020). The effect of vertical ocean mixing on the tropical Atlantic in a coupled global climate model. *Climate Dynamics*, 54(11-12):5089–5109.

Dutton, J. A. (1995). *Dynamics of Atmospheric Motion*. Dover Publications.

Eden, C., Czeschel, L., and Olbers, D. (2014). Toward Energetically Consistent Ocean Models. *Journal of Physical Oceanography*, 44(12):3160–3184.

Efron, B. (1979). Bootstrap Methods: Another Look at the Jackknife. *The Annals of Statistics*, 7(1).

Elipot, S., Lumpkin, R., Perez, R. C., Lilly, J. M., Early, J. J., and Sykulski, A. M. (2016). A global surface drifter data set at hourly resolution. *Journal of Geophysical Research: Oceans*, 121(5):2937–2966.

Fischer, T., Kock, A., Arévalo-Martínez, D. L., Dengler, M., Brandt, P., and Bange, H. W. (2019). Gas exchange estimates in the Peruvian upwelling regime biased by multi-day near-surface stratification. *Biogeosciences*, 16(11):2307–2328.

Fleagle, R. G. and Businger, J. A. (1981). *An Introduction to Atmospheric Physics*. Elsevier Science & Techn.

Flexas, M. M., Thompson, A. F., Torres, H. S., Klein, P., Farrar, J. T., Zhang, H., and Menemenlis, D. (2019). Global Estimates of the Energy Transfer From the Wind to the Ocean, With Emphasis on Near-Inertial Oscillations. *Journal of Geophysical Research: Oceans*, 124(8):5723–5746.

Foltz, G. R., Hummels, R., Dengler, M., Perez, R. C., and Araujo, M. (2020). Vertical Turbulent Cooling of the Mixed Layer in the Atlantic ITCZ and Trade Wind Regions. *Journal of Geophysical Research: Oceans*, 125(2).

Gutjahr, O., Brüggemann, N., Haak, H., Jungclaus, J. H., Putrasahan, D. A., Lohmann, K., and von Storch, J.-S. (2021). Comparison of ocean vertical mixing schemes in the Max Planck Institute Earth System Model (MPI-ESM1.2). *Geoscientific Model Development*, 14(5):2317–2349.

Hans, A. C. and Brandt, P. (2021). Surface drifter data from Meteor cruise M158.

Haza, A. C., D'Asaro, E., Chang, H., Chen, S., Curcic, M., Guigand, C., Huntley, H. S., Jacobs, G., Novelli, G., Özgökmen, T. M., Poje, A. C., Ryan, E., and Shcherbina, A. (2018). Drogue-Loss Detection for Surface Drifters during the Lagrangian Submesoscale Experiment (LASER). *Journal of Atmospheric and Oceanic Technology*, 35(4):705–725.

Heukamp, F., Brandt, P., Dengler, M., Tuchen, F. P., McPhaden, M. J., and Moum, J. N. (2022). Tropical Instability Waves and Wind-Forced Cross-Equatorial Flow in the Central Atlantic Ocean. *Manuscript submitted for publication*.

Hormann, V. and Brandt, P. (2007). Atlantic Equatorial Undercurrent and associated cold tongue variability. *Journal of Geophysical Research*, 112(C6).

Horstmann, J., Borge, J. C. N., Seemann, J., Carrasco, R., and Lund, B. (2015). Wind, Wave, and Current Retrieval Utilizing X-Band Marine Radars. In *Coastal Ocean Observing Systems*, pages 281–304. Elsevier.

Hughes, K. G., Moum, J. N., and Shroyer, E. L. (2020). Evolution of the Velocity Structure in the Diurnal Warm Layer. *Journal of Physical Oceanography*, 50(3):615–631.

Hughes, K. G., Moum, J. N., Shroyer, E. L., and Smyth, W. D. (2021). Stratified shear instabilities in diurnal warm layers. *Journal of Physical Oceanography*.

Hummels, R., Dengler, M., Brandt, P., and Schlundt, M. (2014). Diapycnal heat flux and mixed layer heat budget within the Atlantic Cold Tongue. *Climate Dynamics*, 43(11):3179–3199.

IOC, SCOR, and IAPSO (2010). The international thermodynamic equation of seawater - 2010: Calculation and use of thermodynamic properties. *Intergovernmental Oceanographic Commission, Manuals and Guides*, (56):196 pp.

Jouanno, J., Marin, F., du Penhoat, Y., Sheinbaum, J., and Molines, J.-M. (2011). Seasonal heat balance in the upper 100 m of the equatorial Atlantic Ocean. *Journal of Geophysical Research*, 116(C9).

Koblick, D. (2021). Convert UTC to Solar Apparent Time. https://www.mathworks.com/matlabcentral/fileexchange/32804-convert-utc-to-solar-apparent-time, MATLAB Central File Exchange. Retrieved May 05, 2021.

Kunze, E., Williams, A. J., and Briscoe, M. G. (1990). Observations of shear and vertical stability from a neutrally buoyant float. *Journal of Geophysical Research*, 95(C10):18127.

Large, W. G., Morzel, J., and Crawford, G. B. (1995). Accounting for Surface Wave Distortion of the Marine Wind Profile in Low-Level Ocean Storms Wind Measurements. *Journal of Physical Oceanography*, 25(11):2959–2971.

Lebedev, K. V., Yoshinari, H., Maximenko, N. A., and Hacker, P. W. (2007). YoMaHa'07: Velocity data assessed from trajectories of Argo floats at parking level and at the sea surface.

Lodise, J., Özgökmen, T., Griffa, A., and Berta, M. (2019). Vertical structure of ocean surface currents under high winds from massive arrays of drifters. *Ocean Science*, 15(6):1627–1651.

Lumpkin, R. and Garzoli, S. L. (2005). Near-surface circulation in the Tropical Atlantic Ocean. *Deep Sea Research Part I: Oceanographic Research Papers*, 52(3):495–518.

Lumpkin, R. and Pazos, M. (2007). Measuring surface currents with Surface Velocity Program drifters: the instrument, its data, and some recent results. In Griffa, A., Kirwan, A. D. J., Mariano, A. J., Ozgokmen, T., and Rossby, H. T., editors, *Lagrangian Analysis and Prediction of Coastal and Ocean Dynamics*, pages 39–67. Cambridge University Press.

Masich, J., Kessler, W. S., Cronin, M. F., and Grissom, K. R. (2021). Diurnal Cycles of Near-Surface Currents Across the Tropical Pacific. *Journal of Geophysical Research: Oceans*, 126(4).

Maximenko, N., Niiler, P., Centurioni, L., Rio, M.-H., Melnichenko, O., Chambers, D., Zlotnicki, V., and Galperin, B. (2009). Mean Dynamic Topography of the Ocean Derived from Satellite and Drifting Buoy Data Using Three Different Techniques. *Journal of Atmospheric and Oceanic Technology*, 26(9):1910–1919.

Merckelbach, L., Berger, A., Krahmann, G., Dengler, M., and Carpenter, J. R. (2019). A Dynamic Flight Model for Slocum Gliders and Implications for Turbulence Microstructure Measurements. *Journal of Atmospheric and Oceanic Technology*, 36(2):281–296.

Moum, J., Hughes, K. G., Shroyer, E. L., Smyth, W., Cherian, D., Warner, S. J., Bourlès, B., Brandt, P., and Dengler, M. (2022). Deep cycle turbulence in Atlantic and Pacific cold tongues.

Moum, J. N. and Caldwell, D. R. (1985). Local Influences on Shear-Flow Turbulence in the Equatorial Ocean. *Science*, 230(4723):315–316.

Moum, J. N., Caldwell, D. R., and Paulson, C. A. (1989). Mixing in the equatorial surface layer and thermocline. *Journal of Geophysical Research*, 94(C2):2005.

Moum, J. N., Perlin, A., Nash, J. D., and McPhaden, M. J. (2013). Seasonal sea surface cooling in the equatorial Pacific cold tongue controlled by ocean mixing. *Nature*, 500(7460):64–67.

Niiler, P. P., Sybrandy, A. S., Bi, K., Poulain, P. M., and Bitterman, D. (1995). Measurements of the water-following capability of holey-sock and TRISTAR drifters. *Deep Sea Research Part I: Oceanographic Research Papers*, 42(11-12):1951–1964.

Novelli, G., Guigand, C. M., Cousin, C., Ryan, E. H., Laxague, N. J. M., Dai, H., Haus, B. K., and Özgökmen, T. M. (2017). A Biodegradable Surface Drifter for Ocean Sampling on a Massive Scale. *Journal of Atmospheric and Oceanic Technology*, 34(11):2509–2532.

Ozmidov, R. V. (1965). On the turbulent exchange in a stably stratified ocean. *Izv. Atmos. Oceanic Phys.*, 1(8):853–860.

Pacanowski, R. C. (1987). Effect of equatorial currents on surface wind stress. *J. Phys. Oceanogr.*, 17:833–838.

Peters, H. and Gregg, M. (1988). Some Dynamical and Statistical Properties of Equatorial Turbulence. In *Small-Scale Turbulence and Mixing in the Ocean - Proceedings of the 19th International Liege Colloquium on Ocean Hydrodynamics*, pages 185–200. Elsevier.

Pham, H. T., Sarkar, S., and Winters, K. B. (2013). Large-Eddy Simulation of Deep-Cycle Turbulence in an Equatorial Undercurrent Model. *Journal of Physical Oceanography*, 43(11):2490–2502.

Pham, H. T., Smyth, W. D., Sarkar, S., and Moum, J. N. (2017). Seasonality of Deep Cycle Turbulence in the Eastern Equatorial Pacific. *Journal of Physical Oceanography*, 47(9):2189–2209.

Polzin, K. (1996). Statistics of the Richardson Number: Mixing Models and Finestructure. *Journal of Physical Oceanography*, 26(8):1409–1425.

Polzin, K. L., Garabato, A. C. N., Huussen, T. N., Sloyan, B. M., and Waterman, S. (2014). Finescale parameterizations of turbulent dissipation. *Journal of Geophysical Research: Oceans*, 119(2):1383–1419.

Poulain, P.-M., Centurioni, L., and Özgökmen, T. (2022). Comparing the Currents Measured by CARTHE, CODE and SVP Drifters as a Function of Wind and Wave Conditions in the Southwestern Mediterranean Sea. *Sensors*, 22(1):353.

Price, J. F., Weller, R. A., and Pinkel, R. (1986). Diurnal cycling: Observations and models of the upper ocean response to diurnal heating, cooling, and wind mixing. *Journal of Geophysical Research*, 91(C7):8411.

Rimac, A., von Storch, J.-S., and Eden, C. (2016). The Total Energy Flux Leaving the Ocean's Mixed Layer. *Journal of Physical Oceanography*, 46(6):1885–1900.

Schafstall, J., Dengler, M., Brandt, P., and Bange, H. (2010). Tidal-induced mixing and diapycnal nutrient fluxes in the Mauritanian upwelling region. *Journal of Geophysical Research: Oceans*, 115(C10).

Schneider, N. and Müller, P. (1994). Sensitivity of the Surface Equatorial Ocean to the Parameterization of Vertical Mixing. *Journal of Physical Oceanography*, 24(7):1623–1640.

Smyth, W. D., Hebert, D., and Moum, J. N. (1996). Local ocean response to a multiphase westerly wind burst: 1. dynamic response. *Journal of Geophysical Research: Oceans*, 101(C10):22495–22512.

Smyth, W. D. and Moum, J. N. (2000). Length scales of turbulence in stably stratified mixing layers. *Physics of Fluids*, 12(6):1327–1342.

Smyth, W. D. and Moum, J. N. (2013). Marginal instability and deep cycle turbulence in the eastern equatorial Pacific Ocean. *Geophysical Research Letters*, 40(23):6181–6185.

Smyth, W. D., Moum, J. N., Li, L., and Thorpe, S. A. (2013). Diurnal Shear Instability, the Descent of the Surface Shear Layer, and the Deep Cycle of Equatorial Turbulence. *Journal of Physical Oceanography*, 43(11):2432–2455.

Smyth, W. D., Nash, J. D., and Moum, J. N. (2019). Self-organized criticality in geophysical turbulence. *Scientific Reports*, 9(1).

Smyth, W. D., Warner, S. J., Moum, J. N., Pham, H., and Sarkar, S. (2021). What controls the deep cycle? proxies for equatorial turbulence. *Journal of Physical Oceanography*.

Steger, J. M. and Carton, J. A. (1991). Long waves and eddies in the tropical Atlantic Ocean: 1984–1990. *Journal of Geophysical Research*, 96(C8):15161.

Sutherland, G., Marié, L., Reverdin, G., Christensen, K. H., Broström, G., and Ward, B. (2016). Enhanced Turbulence Associated with the Diurnal Jet in the Ocean Surface Boundary Layer. *Journal of Physical Oceanography*, 46(10):3051–3067.

Sutherland, G., Ward, B., and Christensen, K. H. (2013). Wave-turbulence scaling in the ocean mixed layer. *Ocean Science*, 9(4):597–608.

Thorpe, S. A. and Liu, Z. (2009). Marginal Instability? *Journal of Physical Oceanography*, 39(9):2373–2381.

Wenegrat, J. O. and McPhaden, M. J. (2015). Dynamics of the surface layer diurnal cycle in the equatorial Atlantic Ocean (0°N, 23°W). *Journal of Geophysical Research: Oceans*, 120(1):563–581.

Wenegrat, J. O., McPhaden, M. J., and Lien, R.-C. (2014). Wind stress and near-surface shear in the equatorial Atlantic Ocean. *Geophysical Research Letters*, 41(4):1226–1231.

Wentz, F., Scott, J., Hoffmann, R., Leidner, M., Atlas, R., and Ardizzone, J. (2015). Remote Sensing Systems Cross-Calibrated Multi-Platform (CCMP) 6-hourly ocean vector wind analysis product on 0.25 deg grid, Version 2.0.

Yu, X., Ponte, A. L., Elipot, S., Menemenlis, D., Zaron, E. D., and Abernathey, R. (2019). Surface Kinetic Energy Distributions in the Global Oceans From a High-Resolution Numerical Model and Surface Drifter Observations. *Geophysical Research Letters*, 46(16):9757–9766.

Zappa, C. J., McGillis, W. R., Raymond, P. A., Edson, J. B., Hintsa, E. J., Zemmelink, H. J., Dacey, J. W. H., and Ho, D. T. (2007). Environmental turbulent mixing controls on air-water gas exchange in marine and aquatic systems. *Geophysical Research Letters*, 34(10).

Zippel, S. F., Farrar, J. T., Zappa, C. J., and Plueddemann, A. J. (2022). Parsing the Kinetic Energy Budget of the Ocean Surface Mixed Layer. *Geophysical Research Letters*, 49(2).

List of Figures

Declaration

I confirm that the master thesis *Diurnal cycle of near-surface shear, stratification and mixing in the equatorial Atlantic* is the result of my own work. No other person's work has been used without acknowledgement in the main text of this thesis. This thesis has not been submitted for the award of any other degree or thesis in any other institution.

All sentences or passages quoted in this thesis from other people's work have been specifically acknowledged by clear cross-referencing to author, work and pages. Any illustrations which are not the work of the author of this thesis are specifically acknowledged.

The submitted written version of the thesis corresponds to the version on the electronic storage device (filename: Hans_1103867.pdf).

Place, Date, Signature